



**HAL**  
open science

## The role of the substrate on the mineralization potential of microbial mats in a modern freshwater river (Paris Basin, France).

Adeline Roche, Emmanuelle Vennin, Irina Bundeleva, Anthony Bouton, Dahédrey Payandi-Rolland, Philippe Amiotte-Suchet, Eric C. Gaucher, Hélène Courvoisier, Pieter T. Visscher

### ► To cite this version:

Adeline Roche, Emmanuelle Vennin, Irina Bundeleva, Anthony Bouton, Dahédrey Payandi-Rolland, et al.. The role of the substrate on the mineralization potential of microbial mats in a modern freshwater river (Paris Basin, France).. Minerals, 2019, 9 (6), pp.359. 10.3390/min9060359 . hal-02189495

**HAL Id: hal-02189495**

**<https://hal.science/hal-02189495>**

Submitted on 19 Dec 2020

**HAL** is a multi-disciplinary open access archive for the deposit and dissemination of scientific research documents, whether they are published or not. The documents may come from teaching and research institutions in France or abroad, or from public or private research centers.



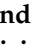

L'archive ouverte pluridisciplinaire **HAL**, est destinée au dépôt et à la diffusion de documents scientifiques de niveau recherche, publiés ou non, émanant des établissements d'enseignement et de recherche français ou étrangers, des laboratoires publics ou privés.



Distributed under a Creative Commons Attribution - NoDerivatives 4.0 International License

Article

# The Role of the Substrate on the Mineralization Potential of Microbial Mats in A Modern Freshwater River (Paris Basin, France)

Adeline Roche <sup>1,\*</sup>, Emmanuelle Vennin <sup>1</sup>, Irina Bundeleva <sup>1</sup>, Anthony Bouton <sup>1</sup>,  
Dahédrey Payandi-Rolland <sup>2</sup>, Philippe Amiotte-Suchet <sup>1</sup>, Eric C. Gaucher <sup>3</sup>,  
Hélène Courvoisier <sup>4</sup> and Pieter T. Visscher <sup>1,5</sup>

<sup>1</sup> Biogéosciences, UMR 6282 CNRS, Université Bourgogne Franche-Comté, 6 Boulevard Gabriel, 21000 Dijon, France; emmanuelle.vennin@u-bourgogne.fr (E.V.); irina.bundeleva@u-bourgogne.fr (I.B.); anthony.bouton@u-bourgogne.fr (A.B.); philippe.amiotte-suchet@u-bourgogne.fr (P.A.-S.); pieter.visscher@uconn.edu (P.T.V.)

<sup>2</sup> GET UMR 5563 CNRS Université de Toulouse, 14 Avenue Édouard Belin, 31400 Toulouse, France; dahedreypayandirolland@hotmail.fr

<sup>3</sup> Total CSTJF, Avenue Larribau, F-64018 Pau Cedex, France; eric.gaucher@total.com

<sup>4</sup> Université Paris-Saclay, CNRS, Neuro-PSI, équipe Communications Acoustiques, Université Paris-Sud, UMR 9197, F-91405 Orsay, France; helene.courvoisier@u-psud.fr

<sup>5</sup> Departments of Marine Sciences & Geosciences, University of Connecticut, Groton, CT 06340, USA

\* Correspondence: adeline.roche@u-bourgogne.fr; Tel.: +33-2080396362

Received: 15 May 2019; Accepted: 11 June 2019; Published: 13 June 2019



**Abstract:** The relationship between environmental conditions and the development, mineralization and preservation of modern tufa microbialites was investigated in a 1.1 km long freshwater stream in Villiers-le-Bâcle, a tributary of Mérentaise river. Detailed mapping of the tufa microbialite distribution combined with sedimentological, petrographical and mineralogical analyses were coupled with chemical measurements. Six organosedimentary structures were identified; their distribution appears heterogeneous along the stream and responds to physicochemical conditions of water and specific biological components (e.g., microorganism, exopolymeric substance). Two of the organosedimentary structures show evidence of mineralization and only one is lithified. Based on field observations and in-situ deployment of mineralization markers (bricks), three zones with increasing mineralization intensities are defined, ranging from no mineralization to thick mineralized crusts forming riverine tufa. Both biotic and abiotic processes were proposed for the tufa microbialite formation. We explained changes in mineralization intensities by the specific physicochemical conditions (e.g., calcite saturation index ( $SI_{calc}$ ) and partial pressure of  $CO_2$  ( $pCO_2$ ) and a closed proximity of the cyanobacterial biofilm and carbonates precipitates. The physical and chemical composition of substrate impact development of microbial communities, mineralization potential of tufa microbialite. Even though the physicochemical and biological conditions were optimal for mineral precipitation, the potential of lithification depended on the presence of a suitable (physical and chemical) substrate.

**Keywords:** continental carbonates; tufa; microbial deposits; precipitation; mineralization

## 1. Introduction

Tufa refers to product of calcium carbonate precipitation under cool, ambient temperature in freshwater [1,2]. Consequently, these carbonate deposits are found in fluvial, lacustrine and palustrine environments. Despite a controversy surrounding the terminology used for tufa in continental settings, this term could be useful for fluvial freshwater carbonate precipitates [3]. The structure and composition

of tufa depends on a complex interplay between physicochemical and biological factors [1,2,4]. Several mechanisms of mineral precipitation have been proposed to explain the formation and deposition of calcium carbonate in freshwater fluvial settings. Whether the origin of tufa is abiotic or biotic remains a controversy [4], it is commonly accepted that specific physicochemical characteristics are required for the formation of tufa, such as the saturation of water with respect of calcite ( $SI_{\text{calc}}$ ), partial pressure of  $\text{CO}_2$  ( $p\text{CO}_2$ ) and the hydrodynamics. Tufa can be also considered as microbialitic when cyanobacterial uptake of  $\text{CO}_2$  through photosynthesis processes predominates the mineral precipitation [5]. However, processes of bio- and organomineralization associated with passive mineralization of organic matter are not usually limited to photosynthesis in natural microbial mats and biofilms, but rather result from the interplay between different metabolisms, including heterotrophic activity [6–8]. As microbial deposits have been preserved in the tufa of the M erantaise tributary, the term “tufa microbialite” is therefore favored here.

The current study focused on the control of the substrate on the formation, distribution and lithification of tufa microbialite. The role of substrate in controlling the origin of the different fabrics such as aphanitic crust, peloid, dendrolites and the resulting mineralization has been discussed extensively, e.g., [4,9]. Gradzinski [10] experimented with tablets in both laboratory and natural settings and (first) discussed the importance of the substrate availability for microbialite development and the presence of additional effective nucleation surfaces by introducing allochthonous biotic components (i.e., algae, housing larvae, mosses, detrital grain, etc.). A presence of a suitable substrate is often mentioned for initiation and growth of microbial deposits but considered as obvious concept. Only a few studies regarded this as a key requirement (factor itself): in marine settings, Stal et al. [11] examined sediment size and availability for microbial mat structure and development, and Ginsburg and Planavsky [12] highlighted the essential role of substrate in the Bahamian microbialites development. Dromart et al. [13] discussed the stability of the substrate as a main factor of development and consequential morphology of Jurassic deep-marine microbial structures. In continental settings, Benson [14] showed how tufa covers the underlying substrate and listed stable substrate among the controlling factors promoting precipitation of the calcium carbonate deposits. Della Porta [3] noticed that distribution of bioherms in Great Salt Lake (USA) was dependent on the presence of a stable substrate. Therefore, a hard, stable, substrate may favor development, growth and preservation of microbial deposits. In addition, the chemical composition of the substrate played a role in the development and mineralization of the tufas as was shown in experiments on substrates of different compositions [10,15–21]. Ultimately, the mineralized microbial mats transform the substrate over time, forming a substrate itself and supporting the development of the successive growing steps (e.g., colonization and growth of successive tufa). Baumgartner et al. [22] and Visscher et al. [23] discussed the role of mat communities and physicochemical conditions on the degree and rate of lithification and production of associated minerals. Biological components (exopolymeric substances (EPS) and microbial cells surfaces such as cyanobacterial filaments) can also act as substrate for nucleation of calcite crystals at microscale [4,7,24–26]. The petrographic components of tufa are mainly composed of micrite, microspar and spar. The biogenic origin of micrite is now commonly described [4,24], but the sparry calcite is more usually considered as inorganic product although frequently observed in association with the biotic micrite [27]. Pedley et al. [28] suggested that the living cyanobacterial sheath is the substrate for crystal formation and that biofilm with EPS are the loci of nanometre-sized spherulites and short-crystal. For Dupraz et al. [29], carbonate nucleation is observed in the EPS and never on the sheath. The organomineralization in EPS is followed by physicochemical precipitation of microsparite and sparite in EPS-free substrate made of micropeloids. If accurate, such ultra-structural properties allow discriminating between biotic and abiotic origins.

The current investigation comprises a multi-scale study of a French river system that supports extensive tufa formation, with a detailed description of the morphological and biological organosedimentary structures. The aim of this study is to unravel influences of external (abiotic, e.g., hydrogeology, hydrodynamics, substrate availability and properties) or internal (biotic, e.g.,

microbial diversity, metabolism and ecological interactions) factors controlling the fluvial carbonate mineralization, with an emphasis on role of the substrate in the development and distribution of the tufa microbialite along the river. Firstly, we will discuss the physical and chemical role of the substrate on tufa microbialite formation and secondly, the role of microbial mats in the development of new available substrate.

## 2. Geographical, Geological and Climatic Context

The study area is located about 20 km southwest from Paris at the northern limit of the Upper Chevreuse Valley Regional Nature Park that is incised by rivers. The Plateau of Saclay is bordered to the north by the Bièvre river, to the southwest by the Mérantaise river and to the south by the Yvette river. The stream investigated in this study, emerges from the Plateau of Saclay and is a tributary of the Mérantaise river (Figure 1). The Plateau of Saclay is composed of the following Oligocene Formations: (1) The “Argiles de Romainville” made up of clays (2–6 m); (2) the “Marnes à huîtres” (4–5 m) and the “Marnes de Brie” both comprising marls (less than 5 m); (3) the “Sables de Fontainebleau” a 65–70 m thick sandstone succession and (4) the less than 10 m thick “Meulière de Montmorency” made up of silts, clays, sands and limestones (Figure 1a; [30]). The climate of the region is temperate with an annual temperature average of 11.2 °C but with significant differences between the coldest and the warmest average monthly temperature (3.9 °C and 19.2 °C, in January and in July, respectively [31]; 1981–2010 observations from Trappes Station, Météo France). The mean precipitation at the site is about 700 mm/yr. The investigated stream is fed mainly by surface and sub-surface flow and by groundwater discharge from two aquifers: (1) A superficial, discontinuous and heterogeneous aquifer, 10 m thick composed of the “Meulière de Montmorency” and (2) a deep, continuous and homogenous aquifer, 50 to 60 m thick, made up of the “Sable de Fontainebleau”. Both aquifers lie above the “Argiles de Romainville”, the “Marnes à huîtres” and the “Marnes de Brie” Formations. The estimated recharge rate of the deep aquifer ranges from 100 to 150 mm/yr depending on hydrograph analysis [32] or 125 to 150 mm/yr based of simulations [33]. The groundwater has a pH value of 7, a conductivity ranging from 459 to 1416  $\mu\text{S}\cdot\text{cm}^{-1}$ , sulfate concentrations ranging from 25 to 332  $\text{mg L}^{-1}$  and nitrate concentrations ranging between 15 and 30  $\text{mg L}^{-1}$  [32,34]. The nitrate inputs originate mainly from agriculture [32]. The sulfate concentrations are explained by the fluid-rock interaction causing the dissolution of celestite or weathering of pyrite in the Fontainebleau sandstones [34].

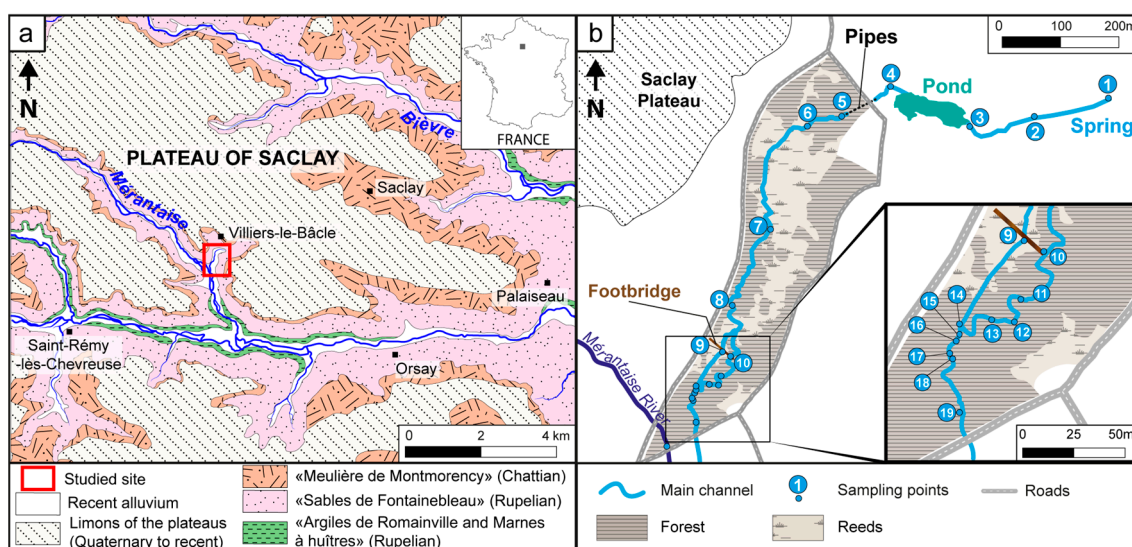


**Figure 1.** (a) Geographic location of the tributary of the Mérantaise River and regional geological map; (b) Detail of the studied stream from the spring to the confluence with Mérantaise with the location of sampling points (1 to 19).



### 3. Materials and Methods

Field campaigns were undertaken in October, November, December 2016, March 2017 and October 2018. Detailed mapping of the bottom sediment, including the presence of benthic microbial communities in river stream was carried out using GPS (Garmin Oregon 450t, Garmin eTrex 30; Garmin (Europe) Limited, Southampton, UK). The mapping effort was accompanied by sampling of the sediments ( $n = 28$ ), microbial biofilms ( $n = 20$ ) and the water column ( $n = 19$ ) covering the length of the stream (Figure 1b). For experimental purposes, 10 terracotta bricks were placed in the streambed in order to measure the potential and rate of mineralization (for 18 months). Seventeen thin sections were (optically) analyzed using polarizing light microscopy (Nikon AZ100; Nikon Corporation, Tokyo, Japan) to determine the petrographic microfacies of microbial mats, biofilms and tufa as well as the nature of the substrate. In addition, parallel samples were dehydrated through a series of ethanol-water solutions and were then critical-point dried in a Leica<sup>®</sup> EM CPD300 apparatus and mounted on stubs before carbon sputtering. The 5 stubs and 5 tufa microbialites were examined using SEM (JSM-IT100, JEOL Ltd, Tokyo, Japan) in order to determine the morphological features of microorganisms and associated minerals. Mineralogical analyzes were performed by X-ray diffraction (XRD) using a Bruker D4 Endeavor diffractometer with  $\text{CuK}\alpha$  radiations combined with a LynxEye detector and Ni filter, under 40kV voltage and 25 mA intensity. Water properties were filtered and measured in the field. The temperature and pH were measured using a WTW pH 3110 with a Sentix<sup>®</sup> 41 electrode (WTW GmbH, Weilheim, Germany); conductivity was determined with a WTW conductimeter cond 3110 (WTW GmbH, Weilheim, Germany), and water velocity were measured with an electromagnetic current meter OTT MF Pro (OTT HydroMet, Germany). Water samples were stored in glass vials kept in refrigerated and transported to the Biogéosciences laboratory. The total alkalinity titration was titrated using the Gran method [35]. Water samples were stored in glass vials kept in refrigerated and transported to the laboratory of Biogéosciences, Université de Bourgogne Franche-Comté, Dijon. Major cation ( $\text{NH}_4^+$ ,  $\text{Na}^+$ ,  $\text{K}^+$ ,  $\text{Mg}^{2+}$  and  $\text{Ca}^{2+}$ ) and anion ( $\text{Cl}^-$ ,  $\text{SO}_4^{2-}$ ,  $\text{NO}_3^-$ ,  $\text{PO}_4^{3-}$ ) concentrations were determined by ion chromatography (Dionex ICS-1500 and DX 100; Thermo Fisher Scientific Corporation) and Dissolved Organic Carbon (DOC) concentration using a Shimadzu TOC-5000A analyzer (Shimadzu Scientific Instruments Inc., Columbia, MD, USA). The PHREEQC Interactive program was used to obtain the calcite saturation index ( $\text{SI}_{\text{calc}}$ ), total dissolved inorganic carbon (TDIC) and partial pressure of  $\text{CO}_2$  ( $\text{pCO}_2$ ) values of water samples [36,37]. Calcite saturation index ( $\text{SI}_{\text{calc}}$ ) was applied as a measure of equilibrium, according to the formula:  $\text{SI} = \log(\text{IAP}/\text{KT})$ , where: IAP—Ion Activity Product for ions forming minerals soluble in the given water solution, calculated according to the law of mass action for the given reaction; KT—equilibrium constant for a given reaction at temperature of sampling.

### 4. Results

Firstly, we will present the physicochemical parameters influencing the organosedimentary structures and the tufa microbialite formation, and secondly, we will focus on the distribution of these structures along the river.

#### 4.1. Physicochemical Parameters of the Stream

##### 4.1.1. Stream Morphology and Associated Vegetation

The physical characteristics presented in Table 1 are arranged by the morphology of the river bed (single or multiple channels, width, depth, and occurrence of topographic breaks) and the water flow velocity. The sedimentary characteristics including the nature and granulometry of the bottom sediment were analyzed according to Wentworth [38]. The presence of plant covers characterized the riverbanks with successive reed beds, dense to clearing forests and grasslands. The dense reed bed coincides with a complex network of multiple channels, which transferred into a single stream in the forests. The main types of vegetation growing in the stream were macroalgae, plants, microalgal biofilms and microbial mats.

**Table 1.** Major characteristics of three zones of the stream; see detailed analyzes in the text below for biological components.

	Zone 1	Zone 2		Zone 3
	No Mineralization	Low Mineralization		High Mineralization
<i>Sampling points</i>	1 to 7	7 to 8; 9 to 10	8 to 9	10 to 19
<i>Distance from spring</i>	0 to 680 m	680 to 840 m	840 to 970 m	970 to 1100 m
	<b>Physical Parameters</b>			
<i>Channel</i>	Single to multiple	Single	Multiple	Single
<i>Depth</i>	Shallow (<10 cm)	Shallow to deep (6 to 30 cm depth)	Shallow (<10 cm)	Shallow to deep (5 cm to 15 cm depth)
<i>Water velocity</i>	Slow (<0.023 m.s <sup>-1</sup> )	Slow to moderate (0.04 to 0.208 m.s <sup>-1</sup> )	Slow to moderate (0.071 to 0.137 m.s <sup>-1</sup> )	Slow to fast (0.025 to 0.585 m.s <sup>-1</sup> )
<i>Topographic break</i>	Pipes	-	-	Dams
<i>Granulometry of bottom sediment</i>	Mud to sand, few pebbles	Mud to pebbles, some blocs	Mud to sand	Mud to blocs
<i>Nature of substrate</i>	Siliceous grains (quartz), wood	Siliceous grains (chert and quartz), woods, roots or anthropogenic (pottery)	Siliceous grains (chert and quartz), wood	Siliceous grains (chert and quartz), wood, roots, anthropogenic (brick, iron, glass)
	<b>Biological Components</b>			
<i>Vegetation</i>	Forest/Reed bed	Forest	Reed bed	Forest clearing
<i>Biofilms, microbial mats</i>	White biofilms; dark gelatinous slime	Dark gelatinous slime; blue-green biofilm; algae	Dark gelatinous slime; few white biofilms; algae	Dark gelatinous slime; brown filaments and EPS-rich mats; blue-green biofilm; algae
	<b>Tufa Microbialite</b>			
<i>Mineralized crusts</i>	None	Thin and patchy	None	Thick and abundant
	<b>Chemical Parameters *</b>			
<i>SI calcite</i>	<u>-1.56 to 0.52</u> ; <b>-0.5</b>	<u>0.89 to 1.13</u> ; <b>0.99</b>		<u>0.75 to 1.27</u> ; <b>1.01</b>
<i>Conductivity (μS.cm<sup>-1</sup>)</i>	<u>547 to 703</u> ; <b>641</b>	<u>668 to 705</u> ; <b>685</b>		<u>644 to 712</u> ; <b>686</b>
<i>pH</i>	<u>6.6 to 7.64</u> ; <b>7.34</b>	<u>8.08 to 8.46</u> ; <b>8.18</b>		<u>7.96 to 8.53</u> ; <b>8.25</b>
<i>pCO<sub>2</sub> (mbar)</i>	<u>26.30 to 3.63</u> ; <b>11.60</b>	<u>2.57 to 0.63</u> ; <b>1.95</b>		<u>3.39 to 0.45</u> ; <b>1.77</b>

\* range is underlined, mean is in **bold**.

#### 4.1.2. Hydrology and Water Chemistry

The hydrochemical data are summarized in Table 2 (see Table S1 for details). The stream water were dominated by HCO<sub>3</sub><sup>-</sup> and Ca<sup>2+</sup>, with concentrations ranging from 128 to 466 mg.L<sup>-1</sup> and from 60 to 150 mg.L<sup>-1</sup>, respectively. The water sample classifies as a Ca-HCO<sub>3</sub> type according to the Piper [39]. The average concentration of the other major elements (Na<sup>+</sup> > Mg<sup>2+</sup> > K<sup>+</sup>; Cl<sup>-</sup> > NO<sub>3</sub><sup>-</sup> > SO<sub>4</sub><sup>2-</sup>) were almost constant all along the stream but showing variation with seasons, with the highest values recorded during the autumn, with the exception of SO<sub>4</sub><sup>2-</sup> (Table S1). Water temperature averages 8.4 °C in November, 6 °C in December and 9.9 °C in March while the mean pH values ranges from 8.19 in November, 8.00 in December and 8.02 in March. The river water was slightly undersaturated with respect to calcite at the spring, and oversaturated all along the stream with SI<sub>calc</sub> values less than 0.8 upstream and above downstream (Figure 2).

**Table 2.** Average of main physicochemical parameters according to the zones (see Table S1 for details).

Zone	pH	Conductivity ( $\mu\text{S}\cdot\text{cm}^{-1}$ )	Alkalinity ( $\text{meq}\cdot\text{L}^{-1}$ )	TOC (ppm)	pCO <sub>2</sub> (mbar)	pCO <sub>2</sub> (x atm. conc.)	Anions ( $\text{mg}\cdot\text{L}^{-1}$ )					Cations ( $\text{mg}\cdot\text{L}^{-1}$ )			IS <sub>calc</sub>	
							Cl <sup>-</sup>	NO <sub>3</sub> <sup>-</sup>	SO <sub>4</sub> <sup>2-</sup>	PO <sub>4</sub> <sup>3-</sup>	HCO <sub>3</sub> <sup>-</sup>	Na <sup>+</sup>	K <sup>+</sup>	Mg <sup>2+</sup>		Ca <sup>2+</sup>
1	7.34	641	4.1	6.34	11.60	29	27.29	23.24	56.78	-	250.1	15.88	2.82	9.76	91.63	-0.5
2	8.18	685	5.38	6.17	1.95	5	27.01	38.22	50.20	-	328.15	15.39	3.28	11.33	115.75	0.99
3	8.25	686	5.04	6.14	1.77	4	27.71	47.64	45.59	-	307.24	16.25	2.72	11.85	121.72	1.01

(-) no data.

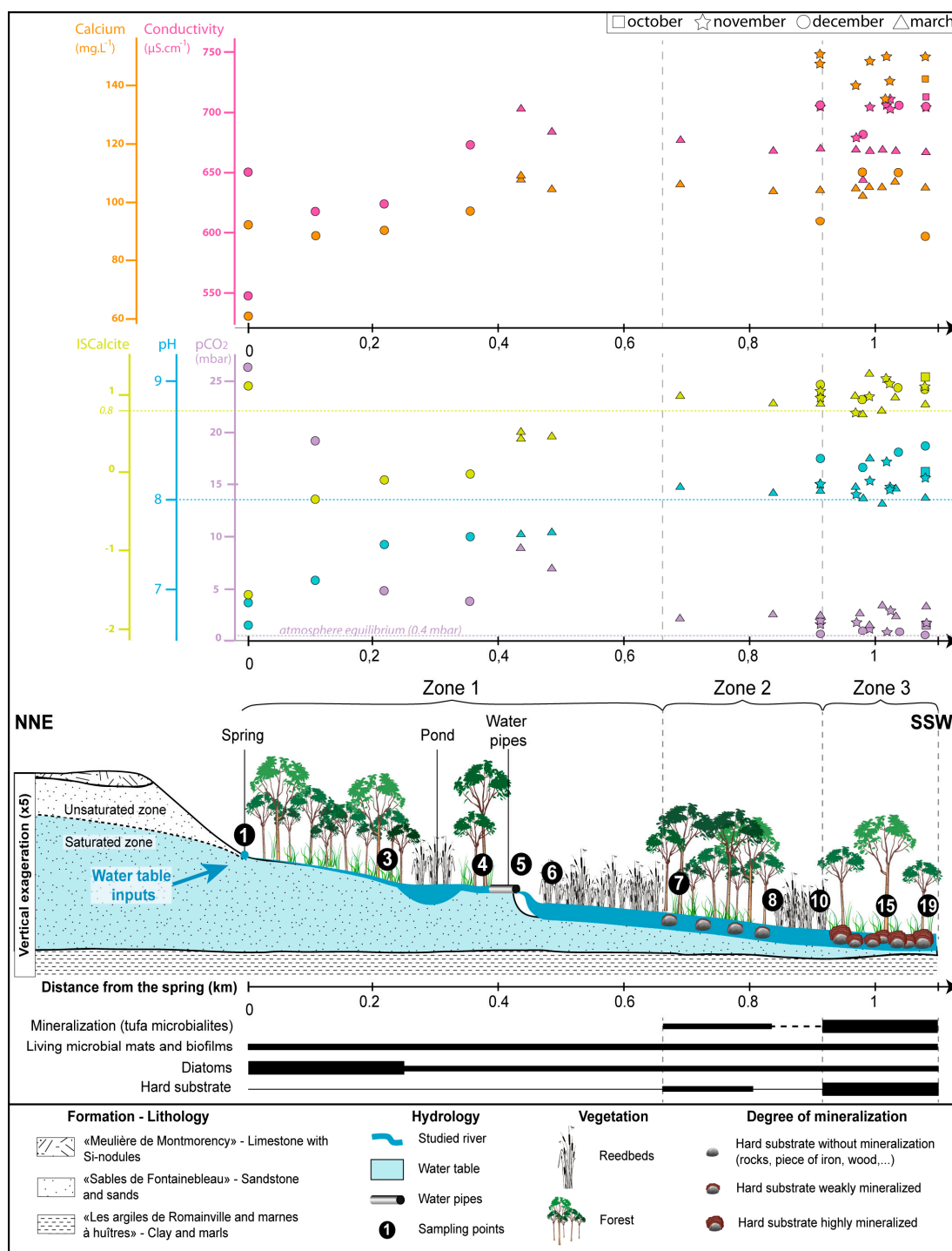


**Figure 2.** 2D profile of stream showing main hydrochemical characteristics ( $IS_{calc}$ ; pH;  $pCO_2$ ; calcium concentration; conductivity; the color of symbols corresponds to the color of the axes of the various hydrochemical variables and shapes of the symbols show the time of the year; mapping of biological (type of vegetation, microbial mats and biofilms, diatoms) and sedimentary (tufa microbialites, hard substrate) characteristics all along the stream.

## 4.2. Organosedimentary Structures

### 4.2.1. Microbial Mats and Biofilms

The term microbial mat is used here for vertically laminated organosedimentary structures developing on solid surfaces, embedded in an organic extracellular matrix [11,22,40,41]. In contrast, ‘biofilms’ are considered here as non-structured, single microbial laminae embedded in extrapolymeric substances (EPS) [42,43] bound to a solid surface [44]. The distribution of biofilms and microbial mats responding to average hydraulic pattern may be considered as “biofilm catena” [45].

Five types of microbial mats and biofilms were identified in the present study: (1) white biofilms, (2) dark gelatinous slime, (3) filament-rich clusters (4) brown filaments and EPS-rich mats, and (5) blue–green biofilms. They are organized following a “biofilm-catena” distribution [45]: Low-energy setting (1 and 2), moderate to high-energy setting (3 and 4) and high-energy settings (5). (1) The white biofilms were composed of diatoms, cyanobacteria and EPS, which developed on the water surface in the upstream part of the stream (between points 1 and 3, Figure 2) during cooler seasons (Figure 3a). Similar biofilms have been reported and can result from abiotic or biotic sulfide oxidation. Sulfate reducers respire organic carbon produced by diatoms and/or cyanobacteria, producing sulfide. Consecutively, the sulfide is oxidized, either biotically (e.g., by filamentous or unicellular colorless sulfur bacteria; the former were not observed in the current investigation) or abiotically (by atmospheric O<sub>2</sub> at the water-air interface) [46,47]. (2) The 2–10 cm-thick dark gelatinous slime was a non-mineralized, flat and smooth, dark brown mat characterized by a copious amounts of EPS (Figure 3b). Similar gelatinous structures resulted from excessive EPS production by microbial communities generated due to environmental cues [7,40,42,48]. The thickness (mm to dm-thick) of these structures increased from the spring to the distal part of the stream. (3) The filament-rich clusters were composed of sub to mm-long microbial filaments forming non-mineralized, non-cohesive clusters that developed downstream mainly during the autumn. These submersed structures were systematically attached on a hard substrate, hanging down in cavities beneath or on the side of pebbles, granules and boulders (Figure 3c). (4) Brown filamentous EPS-rich mats were composed of mm-long filaments organized in patchy bunches were attached to hard substrate surfaces on which they developed during the autumn in moderate-energy settings (Figure 3d). These mats had internal laminations comprising black filaments, diatoms, organic matter, framboidal pyrite and quartz. Diatoms, belonging to the genus *Gyrosigma* [49], were common at the surface of the mat (Figure 3e). The mineral fraction of the mat included calcite-rich peloids and rhombs. (5) The blue–green biofilms constituted a hard thin blue–green lamina overlying a carbonated layer (Figure 3f). The blue–green biofilms developed downstream in the central more hydrodynamic areas of the channel. A continuous mineral crust within the biofilm covered the surface of the hard substrates that correspond frequently to tufa microbialites. They were made up of microbial filaments associated with larval housings (i.e., *Trichoptera* pupal cases) and diatoms identified as *Cocconeis* sp.; *Navicula* sp. and *Amphora pediculus* [49] (Figure 3g). Experiments with the terracotta bricks revealed that mineralization started in isolated small hemispheroids (submm-thick) that fused laterally to form continuous mm to cm-thick layers. The brown filamentous mats and blue–green biofilms were only observed overlying the surface of tufa microbialite described below.

### 4.2.2. Tufa Microbialites

Tufa microbialites observed in this study comprised mineralized carbonate crusts arranged in mm-thick laminae composed of either isolated or bunched filament molds and sheath remnants embedded in a micritic to microsparitic matrix. The tufa microbialites developed on various substrates and mimic that substrate’s morphology. Their fabrics were composed of flat or slightly wavy laminae with a thickness of 100 to 1000 μm-thick (Figure 3h,i). The identification of the fabrics in thin sections, based on their morphology, matrix and the associated biotic and abiotic components (Table 3), allowed to classify five microfabrics: (1) Dense or (2) loose filament molds; (3) clastic-rich laminae; (4) micritic-rich laminae; and (5) iron-rich laminae.



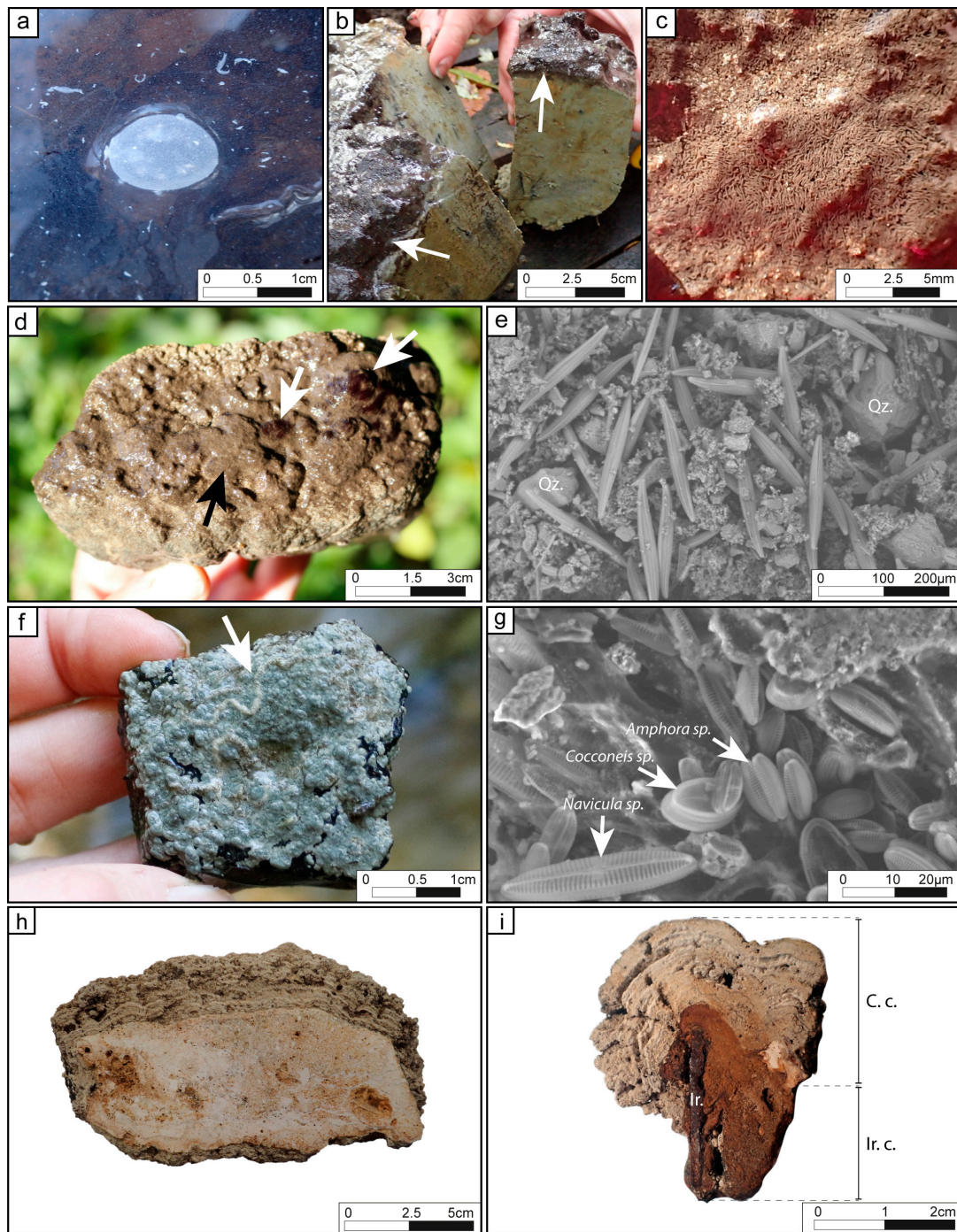


**Figure 3.** Organosedimentary structures observed in the stream. (a) White biofilms trapping a bubble at the water–air interface; (b) dark gelatinous slime (white arrows) overlying a muddy bottom sediment; (c) filament-rich clusters in cavities and on edges of gravels; (d) brown filaments (white arrows) and EPS-rich mats (black arrow) covering tufa microbialite; (e) SEM top view of brown filaments and diatoms of genus *Gyrosigma* (with copious amounts of EPS), and quartz grains (Qz) embedded in exopolymeric substance (EPS); (f) blue–green biofilms with larval housings (white arrow) forming meandering pattern covering tufa microbialite; (g) SEM view of blue–green biofilms covered by three genera of diatoms (*Navicula*, *Cocconeis*, *Amphora*); (h) cross-section of tufa microbialite on siliceous substrate showing alternation of mm-thick laminae; (i) cross-section of tufa microbialite on ferrous substrate (Ir.) covered by an iron crusts (ir. c.) and a carbonated crust (C. c.) composed of alternations of laminae.

Table 3. Microfabrics.

Microfabrics	Morphology of Laminae	Matrix	Main Components of Laminae	Other Components	Preservation/Porosity	Substrate	Biological Affinity	Figures
Dense filamentous	Flat or slightly wavy laminae (100 to 1000 $\mu\text{m}$ thick), composed of hemispheroid and fan-shaped structures, frequently sharply truncated by dissolution surface.	Microsparite or light micrite.	Molds of filaments organized in fan-shaped and erected perpendicular to the basement. Composed of two-size types of filaments: 12 to 13 $\mu\text{m}$ in diameter filaments slightly arched and 500 $\mu\text{m}$ long. Segmentation may be observed every 17 to 23 $\mu\text{m}$ ; 2–4 $\mu\text{m}$ in diameter straight filaments with and 25 to 100 $\mu\text{m}$ long. Molds are empty or filled by dark matrix (oxides?). In MEB view, remnants sheath preserved in filaments molds.	Scarce detrital grains (quartz, K-feldspars, plagioclases; 100 to 200 $\mu\text{m}$ ) trapped in the residual porosity between the filaments; scarce circles shapes (Chlorellopsis-like?) with a diameter ranging from 50 to 100 $\mu\text{m}$ within or at the top of laminations; few oxides crystals (from 10 to 30 $\mu\text{m}$ -width); larval housings, <i>Trichoptera</i> pupal cases and diatoms.	Large vuggy to interparticular porosity; dissolution cavity is filled by detrital grains.	Micritic laminae, loose filaments laminae. Boulders of different composition.	Thick filaments: <i>Phormidium</i> (?) Thin filaments: <i>Leptolyngbya</i> sp.	Figures 4a–d, and 6d
Loose filamentous	Flat to wavy laminae from 100 to 900 $\mu\text{m}$ -thick, sometimes showing fan-shaped structures or concentric organization; interlayered with micritic laminae with planar laminations of different colors; laminae are frequently sharply truncated by dissolution surfaces.	Dense micrite, locally clotted.	Molds of scattered straight filaments branching or not with diameters from 4 $\mu\text{m}$ to 10 $\mu\text{m}$ and 10 to 100 $\mu\text{m}$ long; isolated filaments embedded in micritic matrix with local clotted organization; walls highlighted by dark lines or filled by a dark matrix; filaments are perpendicular to substrate or disorganized. In MEB view, remnant sheath preserved in filaments molds.	Few oxides crystals (10 to 40 $\mu\text{m}$ ); diatoms.	Weak vuggy porosity.	Dense filaments laminae, micritic laminae with or without quartz. Boulders of different composition.	<i>Phormidium</i> sp.	Figures 4f,g, and 6d
Clastic-rich	300 to 800 $\mu\text{m}$ -thick discontinuous or continuous laminae, with dark rims at the top and dissolution surfaces.	Micritic or light microsparite.	Peloids, angular and unsorted quartz 30 to 100 $\mu\text{m}$ , scarce K-feldspars or plagioclases.	Rare disorganized thin molds of filaments (4 to 6 $\mu\text{m}$ ).	Strong to weak vuggy porosity.	Iron-rich laminae with quartz, chert.	-	Figure 6a

Table 3. Cont.

Microfabrics	Morphology of Laminae	Matrix	Main Components of Laminae	Other Components	Preservation/Porosity	Substrate	Biological Affinity	Figures
Micritic	Wavy laminae from 30 to 300 $\mu\text{m}$ -thick, top are often limited by dark rims and dissolution surfaces.	Micritic or light microsparite.	Homogeneous dense micrite, lined by black rims enriched in iron (?).	Few oxide crystals (20 to 120 $\mu\text{m}$ ).	-	Mainly in contact with the boulders; dense filament laminae; iron-rich laminae with or without quartz.	-	Figure 6b,c
without quartz	30 to 100 $\mu\text{m}$ -thick laminae, with thin $\mu\text{m}$ -thick wavy laminations.	Dark brown micrite or microsparite.	Dense dark matrix composed of goethite and siderite (?).	Small oxide crystals (20 to 40 $\mu\text{m}$ ).	No porosity	Micritic laminae with quartz, iron, chert.	-	
Iron-rich with quartz	100 to 500 $\mu\text{m}$ -thick laminae; delimited by irregular and black rims and dissolution surfaces.	Dark clotted micrite, grey micrite or microsparite.	Dense dark matrix composed of goethite and siderite (?); peloids, angular and unsorted quartz (20 $\mu\text{m}$ to 300 $\mu\text{m}$ ) trapped in the matrix, scarce K-feldspars, plagioclase or siliceous-rich fragments.	Oxide crystals (10 to 30 $\mu\text{m}$ ), rare wood fragments.	No porosity	Micritic laminae with quartz, chert, wood.	-	Figure 6b,d

(1) Dense filamentous laminae: The laminae appeared flat or slightly wavy with a thickness of 100 to 1000  $\mu\text{m}$ , which were composed of filamentous molds embedded in calcitic microsparite or micrite. Molds were either empty or filled with organic sheaths or oxides (Figure 4a). The erected non-branching filaments were organized in a fan-shaped pattern and attached on hard substrates, comprising previously deposited microbial laminae. These hemispheroid structures were usually covered by a blue–green biofilm. Thick and thin filaments were present in close proximity of each other (Table 3): (i) 12 to 13  $\mu\text{m}$ -diameter, arched filaments displayed locally preserved evidence of segmentation (Figure 4b). Their characteristics suggested that they could be assimilated to *Phormidium incrustatum* [50] or *Homeothrix/Calothrix* [51]; (ii) 2 to 4  $\mu\text{m}$ -diameter straight filaments with no segmentation and an appearance similar to the non-heterocystous cyanobacteria *Leptolyngbya* sp. [51,52]. These laminae often showed high porosity due to open spaces between the filaments and the fan-shaped structures. Pores were filled in with micrite, microsparite and clastic materials. The surface of these laminae was frequently truncated or dissolved and showed evidence of trapped detrital grains (quartz and feldspars) or oxides. Some circular shapes with a diameter ranging from 50 to 100  $\mu\text{m}$  were trapped in the fabric (Figure 4c). Similar fabric morphologies have been observed in Eocene Green River Formation, and were interpreted as green algae *Chlorellopsis coloniata* Reis, fungal spores or insect eggs [53]. Larval housings, forming rounded and elliptical shapes in cross-section [17,50] (Figure 4d), diatoms and *Trichoptera* pupal cases were usually attached to the surface laminae and substrate (Figure 4e), but also locally trapped within the laminae.

(2) Loose filamentous laminae: These laminae, with a thickness of 100 to 900  $\mu\text{m}$ , were either well-defined flat, wavy and concentric in shape (Figure 4f,g), frequently sharply truncated and dissolved. They were mostly composed of a calcitic micritic matrix, locally clotted with embedded filaments (Figure 4f). The molds of filaments were scarce and isolated but easily recognizable due to oxide fillings (Figure 4f). The straight filaments, which were 4 to 10  $\mu\text{m}$  in diameter, were either arranged vertically from the basement surface, subparallel to the depositional surface or disorganized. The filaments resembled the cyanobacteria *Phormidium* sp., frequently observed in modern tufa-depositing rivers, e.g., [17,18,52,54,55]. In addition, oxides and diatoms were occasionally observed.

Both dense and loose filamentous laminae exhibited similar microstructures and mineral fabrics. Scanning electron microscopic observations revealed that filaments were completely encrusted in a carbonated matrix (Figure 5a), covered by calcite lamellas and embedded in a calcitic matrix, mostly composed of microsparite or micrite. The presence of previously formed filaments was discernible by the segmented sheath remains or hollow tubes within matrix (Figure 5a). Between filaments, the fabric was composed of micropeloids, dendrites, and rhombs. The micropeloids (up to 40  $\mu\text{m}$  in diameter; Figure 5b) were made up of aggregates of nanospheres with diameter ranging from 100 to 200 nm (Figure 5c). The dendrites presented  $\mu\text{m}$ -long acicular crystals assembled in three diverging directions forming pyramidal structures or Christmas tree-like (Figure 5d). Rhombohedral polyhedra were composed of triangular masses with iso-oriented assemblage of 0.5  $\mu\text{m}$ -long trigonal. Their edges measured from 7 to 17  $\mu\text{m}$ . These polyhedra agglutinated in the same direction forming larger triangular polyhedra (Figure 5e,f).

(3) Clastic-rich laminae: Showed well-defined, 300 to 800  $\mu\text{m}$ -thick, flat laminae. They were composed of scarce 4 to 10  $\mu\text{m}$ -thick filament molds, peloids, angular and sorted quartz as well as feldspars (Table 3). The surfaces were frequently affected by dissolution, and covered by an oxide-rich rim (Figure 6a). The clastic-rich laminae showed a similar composition and organization as the unconsolidated brown filamentous mats.

(4) Micritic laminae: The discontinuous to continuous, 30 to 300  $\mu\text{m}$ -thick laminae were composed of a dense homogenous micrite lacking inclusions, with the exceptions of a few small oxides crystals. The wavy surface often showed strong dissolution rims with oxide-rich crusts (Figure 6b,c).



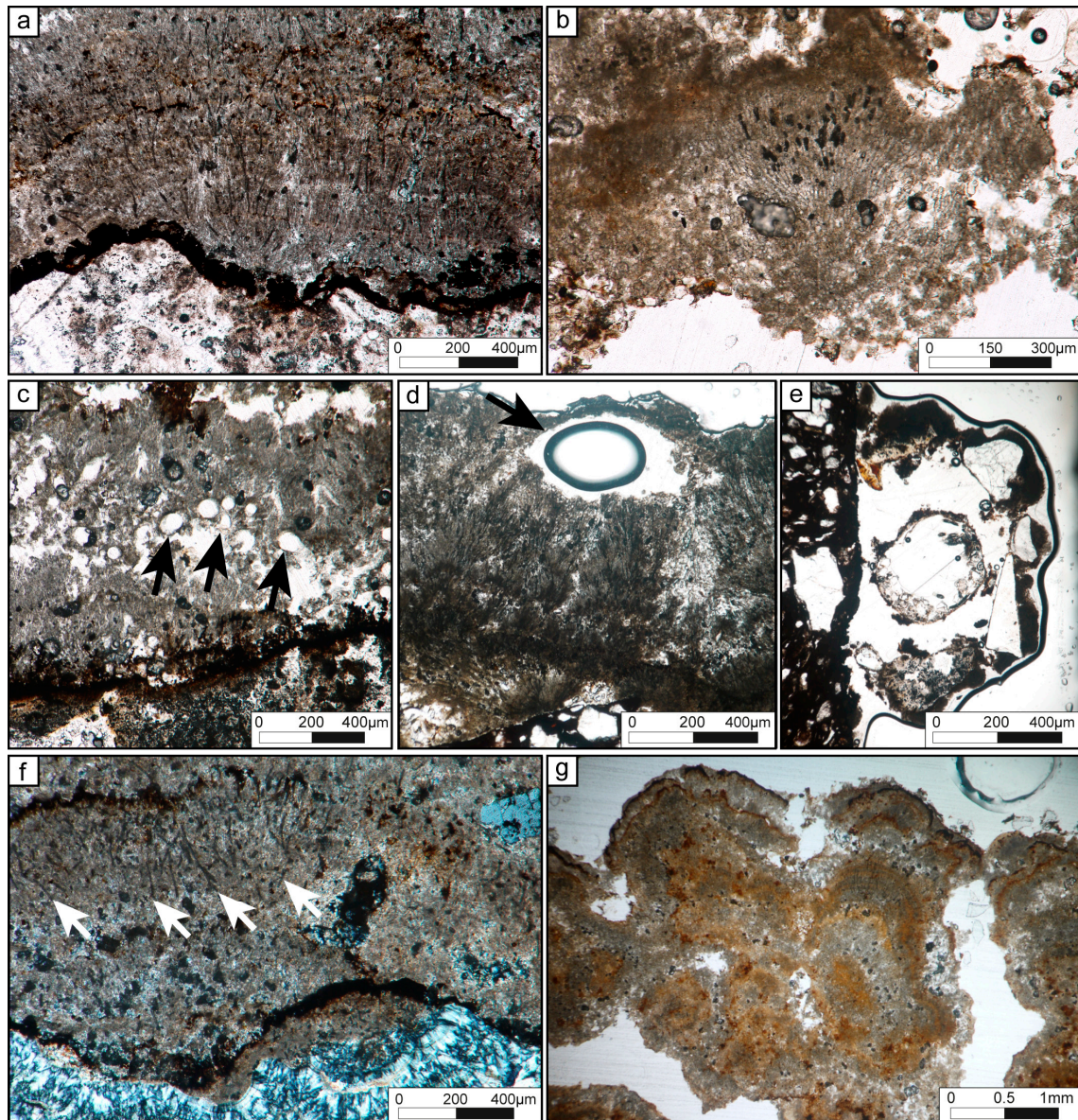


**Figure 4.** Filamentous-rich microfabrics in thin section view. (a) Dense filamentous lamina covering a siliceous substrate; (b) segmented filaments forming fan-shaped structures in dense filamentous lamina; (c) circle shapes (black arrows) within a dense filamentous lamina; (d) cross-section of a larval housing (black arrow) near the surface of a dense filamentous lamina; (e) cross-section of *Trichoptera* pupal cases on the edges of substrate; (f) wavy loose filamentous laminae consisting of isolated filaments (white arrows); (g) loose filamentous laminae composed of concentric structures and isolated filaments.



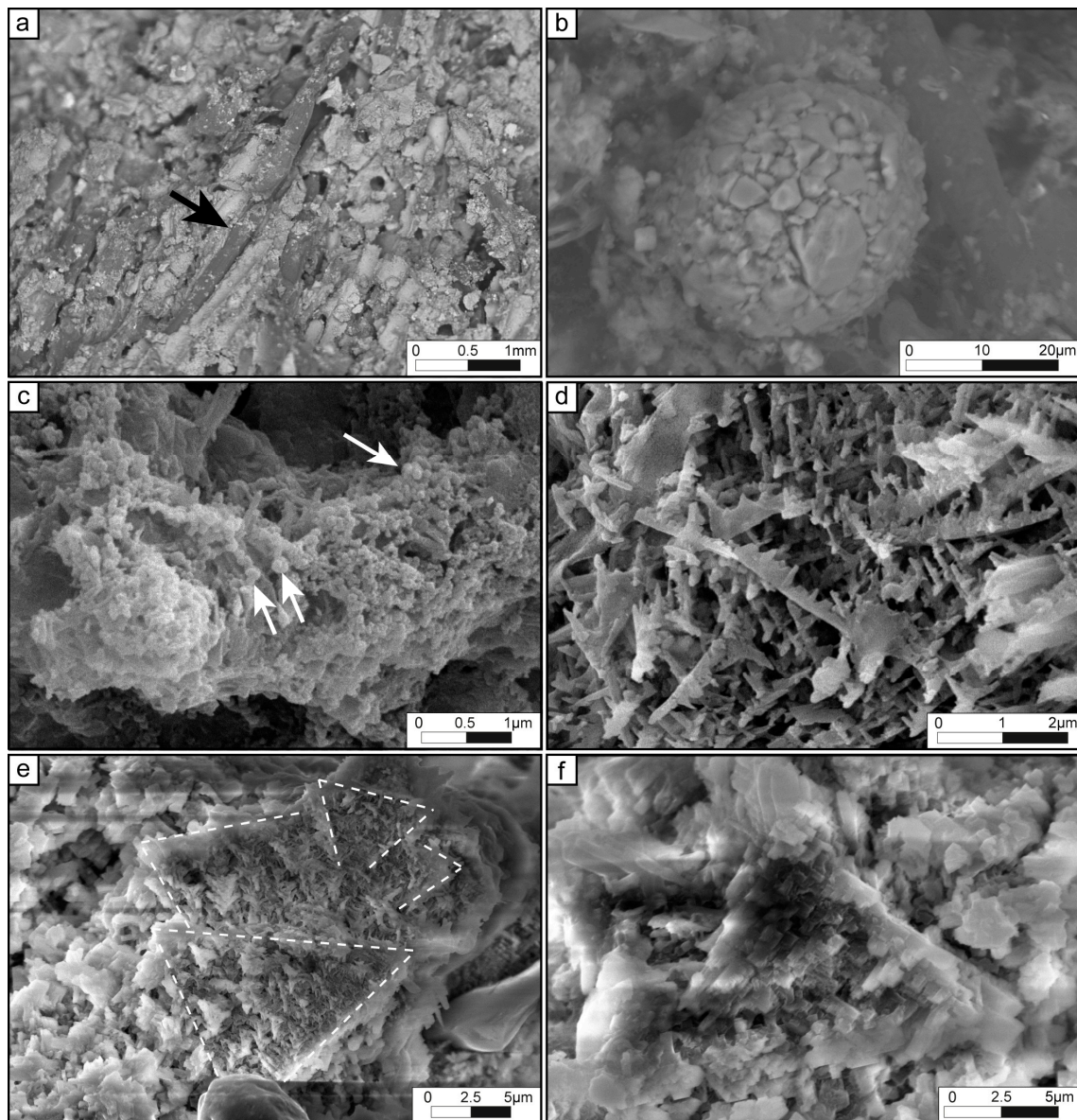


**Figure 5.** Microstructures of tufa microbialite in SEM view. (a) Remnants of sheaths of filamentous cyanobacteria (*Phormidium* sp.; black arrow) embedded in carbonate matrix; (b) micro-peloids composed of carbonate grains; (c) aggregates of nanospheres (white arrows); (d) dendrites formed by long acicular crystals; (e) trigonal polyhedra and (f) rhombohedra forming triangular masses.

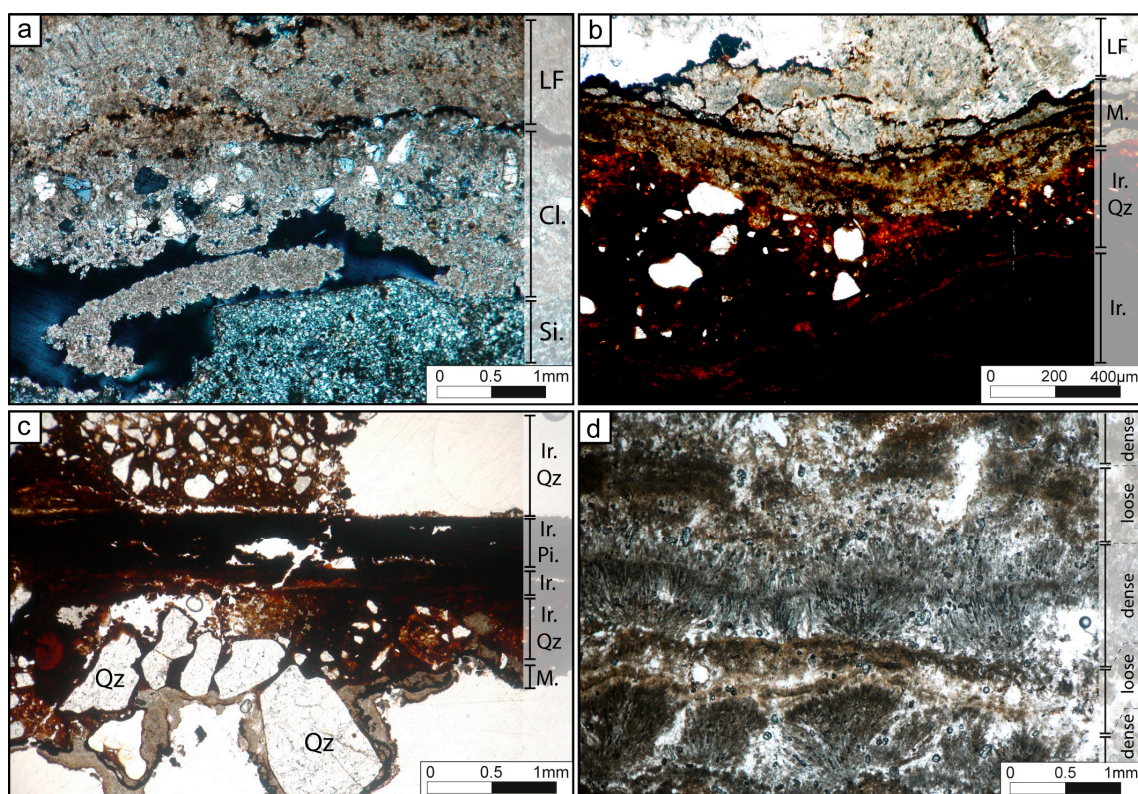


**Figure 6.** Microfabrics of tufa microbialites in thin section view. (a) Clastic-rich lamina (Cl.), composed of detrital grains embedded in microsparite and separated from loose filamentous laminae (LF) by a dark dissolution rim, overlying a siliceous substrate (Si.); (b) succession of iron-rich laminae without quartz (Ir.), and with quartz (Ir. Qz), micritic laminae (M.) and loose filamentous laminae (LF); (c) fragment of iron (Ir. Pi.) surrounded by iron-rich laminae (Ir.), iron-rich laminae with quartz grains (Ir.Qz) covered by two micritic laminae (M.); (d) alternation of dense and loose filamentous laminae.

(5) Iron-rich laminae: 30 to 500  $\mu\text{m}$ -thick iron-rich laminae with  $\mu\text{m}$ -thin goethite ( $\text{FeO}(\text{OH})$ ) and siderite (?;  $\text{FeCO}_3$ ) accumulations. These laminae occasionally contained quartz (Figure 6b,c). Both angular and unsorted quartz were observed combined with a few feldspar and/or quartz grains (Table 3). These laminae were only formed in contact with larger iron fragments, e.g., nail (Figure 6c).

The most representative tufa microbialites along the river are composed of couplets made of dense and loose filamentous laminae (1 and 2; Figure 6d). In all samples including those obtained from the terracotta bricks, micritic laminae at the surface of the underlying hard substrate were almost systematically developed forming the base of the tufa microbialites.

#### 4.3. Zonation of the Mineralization Intensity

Field observations along the stream and experiments using terracotta bricks formed the basis for subdividing the 1.1 km-long river into three zones depending on the mineralization intensity of the organosedimentary structures. Each of these zones displays different physical, sedimentary, biological and hydrochemical characteristics (Figures 2 and 7; Tables 1 and 2).



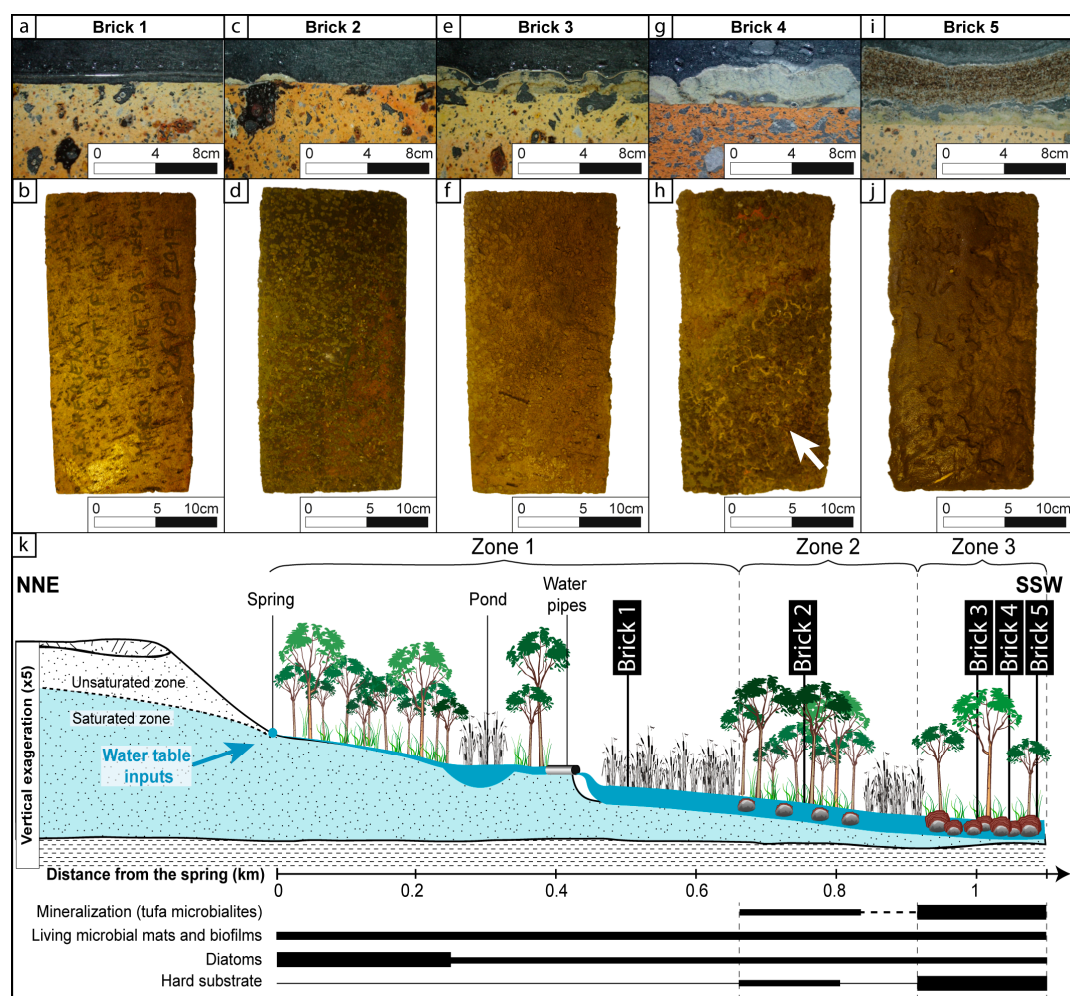


**Figure 7.** Degree of mineralization along the stream (a,c,e,g,i): Thin section view of terracotta bricks; (b,d,f,h,j): Top view of terracotta bricks; (a,b) No mineralization on top brick 1 (Zone 1); (c) and (d) thin and patchy tufa microbialite on top of brick 2 (Zone 2; forest-dominated); (e,f) thin and continuous tufa microbialite on brick 3 (Zone 3); (g,h) continuous and thicker tufa microbialite and blue-green biofilms (white arrow) on brick 4 (Zone 3); (i,j) mm-thick tufa microbialite covered by dark gelatinous slime on brick 5 (Zone 3); (k) 2D-profile of the stream with location of terracotta bricks (see captions Figure 2).

#### 4.3.1. Zone 1: No Mineralization

Zone 1 extends from the spring to where the vegetation transitioned from a reed bed to a forest (points 1 to 7; Figure 2). This zone is characterized by slow-flowing water in a single shallow channel (water depth around 10–20 cm high water-level; Figure 8a). After 200 m, the water flows in a 120 m-long and 200 m-wide, approximately one-meter-deep pond (Figure 8b). Downstream of the pond, water is directed into two channels, the first approximately 10 m-long one (Figure 8c) and the second an 80 m long. The channels are associated with a topographic break (terrace) of about 2 m in height causing a turbulent zone (Figure 8d). A thick deposit of dead leaves covered the river bottom. The bottom sediment underneath the leaves was mostly composed of mud-sized sediments with a lower contribution of granules (quartz grains). The clay assemblage was similar along the entire streambed and consisted of vermiculite (29%), kaolinite (27%), interstratified illite-smectite (25%), illite (12%) and chlorite (8%). Downstream, the main channel branches into several very shallow watercourses without topographic breaks, crossing a dense herbaceous reed bed area (from points 5 to 7; Figure 2). In this part of zone 1, the substrate was still composed of fine particles from mud to siliceous sand

(Figure 8e). In the entire zone, pH values were the lowest and increase gradually downstream from 6.6 to 7.6. The  $p\text{CO}_2$  values are inversely proportional to pH values with the highest values during the spring (26.3 mbar; 66 times more elevated than the atmospheric concentration (0.4 mbar), point 1; Table S1; Figure 2). Conductivity, alkalinity and  $\text{SI}_{\text{calc}}$  measurements gradually increase downstream (Table S1; Figure 2). White biofilms at the water-air interface (Figures 3a and 8a) and dark gelatinous slimes resting on the bottom of the stream were frequently observed. However, no tufa microbialite was found in this zone, not even when terracotta bricks were deployed as hard surface (brick 1; Figure 7a,b). Instead, the bricks were covered locally by *Trichoptera* pupal cases. No mineralization of any of the organosedimentary structures was observed in this zone.

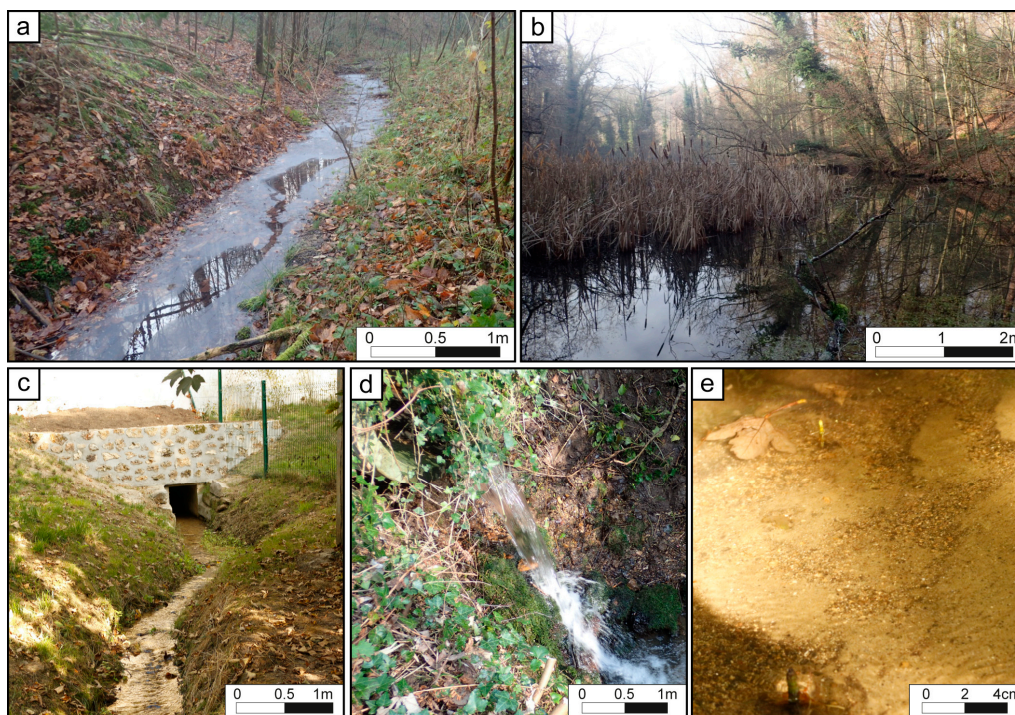


**Figure 8.** Main characteristics of Zone 1 from the spring to the forest (see Figure 2 for exact location). (a) Single channel extending from the spring to the pond with a white biofilm covering the water–air interface; (b) pond colonized by reeds; (c) culvert; (d) waterfall with a meter-high topographic break caused by the culvert; (e) fine-grained, mud-silt sized bottom sediment.

#### 4.3.2. Zone 2: Low Mineralization

Zone 2 encompassed a forested area interrupted locally by a reed bed (points 7 to 10; Figures 2 and 9a,b). In this zone, tufa microbialite with a low degree of mineralization first appeared. The forest area (points 7 to 8; Figure 2) with bushy vegetation was crossed-cut by a single deeper channel (around 30 cm deep) with a several shallow topographic breaks (Figure 9a). The sand-sized bottom sediment was coarser than in Zone 1; the finest particles still comprised muds but the largest particles reached boulder-size (Figure 9c,d). The streambed also contained wood fragments, roots and anthropic debris like pottery. Downstream, the forest passed through a second reed bed (points 8 to 10; Figure 2), in which the stream divided again into multiple, shallow channels without topographic breaks. The entire zone was characterized by a downstream increase in pH from 7 to 8 and  $p\text{CO}_2$  values ranging between 0.63 and 2.57 mbar (Figure 2), meaning that the lower values are almost at equilibrium with atmosphere. In this zone, dark gelatinous slimes covered the bottom of the river at the edges of the channel (Figure 9e,f) and white biofilms accumulated at the water-air interface (Figure 9g), where hydrodynamic conditions were lower and consequently the sediments softer and thinner (mud to silt; Figure 3b). Low mineralization was observed on brick 2 with the development of patchy and less than



mm-thick micritic laminae with loose filamentous (Figure 7c,d). The terracotta brick was colonized by *Trichoptera* pupal cases on the edges (Figure 4e). In addition, thin tufa microbialites developed on pebbles, cobbles and boulders of different lithology (Figure 9h). These tufas were associated with blue–green biofilms during the warmer period of the year and localized in the area with the highest hydrodynamic conditions (Figure 9i).

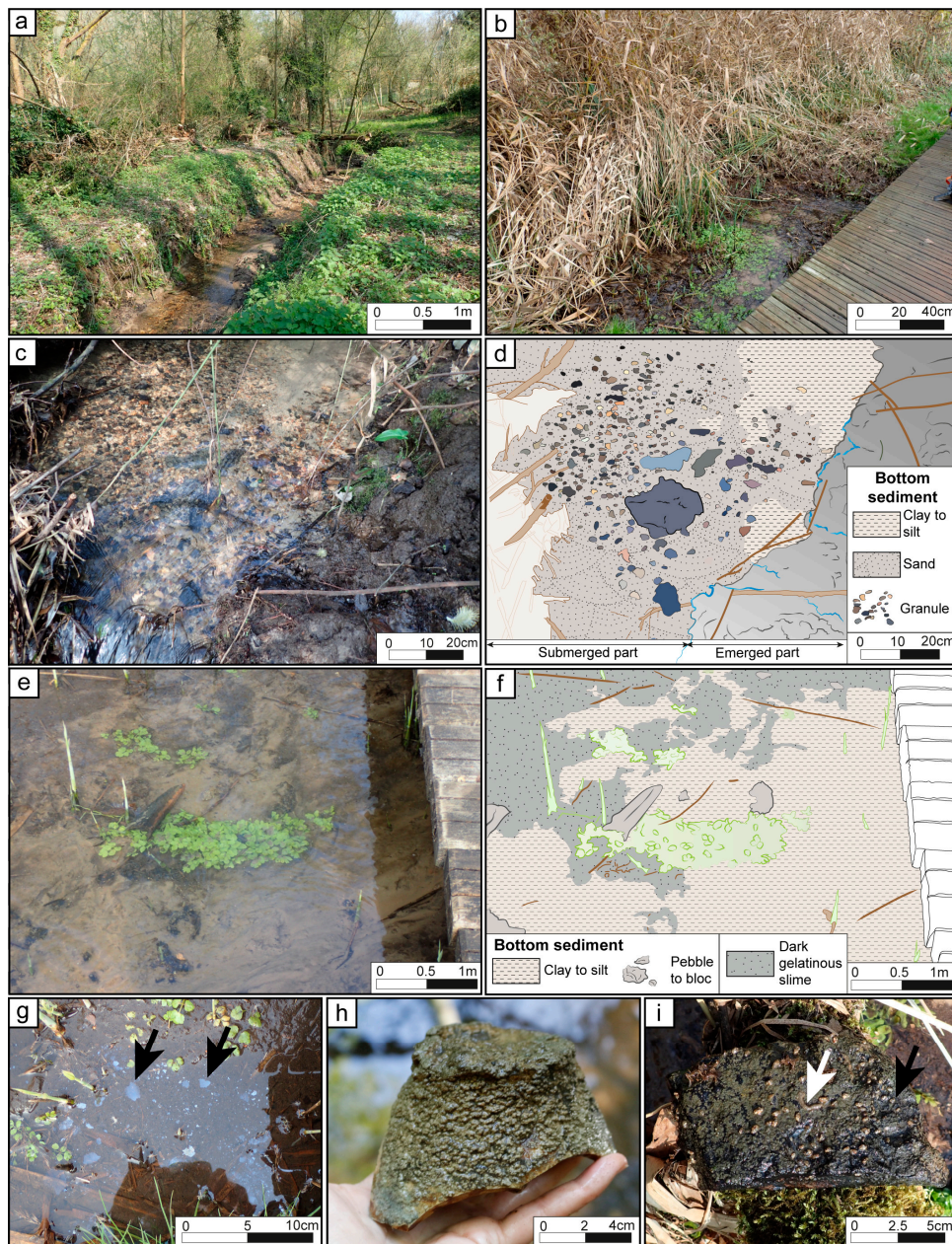


**Figure 9.** Main characteristics of Zone 2 from the forest to the footbridge (see Figure 2 for exact location). (a) Single, deep (70 cm to 1 m) channel in the forest-dominated zone; (b) shallow (less than 15 cm) multiple channels flowing through the reed bed; (c) view and (d) drawing of the bottom sediments of the forest-zone dominated by sand size; (e) view and (f) drawing of the bottom sediment of the zone reed-dominated by mud to silt size with few pebble and blocks, dark gelatinous slime covering soft substrate; (g) patchy white biofilms in the reed bed zone (black arrows); (h) fragment of pottery covered by a mm-thick pustular tufa microbialite; (i) substrate covered by thin, patchy blue–green biofilms with *Trichoptera* pupal cases (black arrow) and larval housings (white arrow).



#### 4.3.3. Zone 3: High Mineralization

Zone 3 initiated in a clearing part of the forest (points 10 to 19; Figure 2), where the previously-formed multiple channels regrouped into a fast-flowing single stream, less than half meter deep (Figure 10a–c). Several small topographic breaks provided local turbulence. The average particle size of the bottom sediment was dominated by coarse sand to gravel with a granulometry ranging from muds to boulders (Figure 10a,b). The sediment composition varied from silica (Figure 3h), wood fragments (Figure 10d), roots to anthropic substrates like pieces of iron (Figures 3i and 10e), and glass fragments (Figure 10f,g). In term of chemical composition of the water, Zone 3 exhibited lower  $p\text{CO}_2$  values (ranging between 0.44 and 3.4 mbar), higher pH values (around 8.6) and  $\text{SI}_{\text{calc}}$  (around 1.27). The lowest value of  $p\text{CO}_2$  corresponds to a complete return to the atmospheric equilibrium. This area revealed the presence of abundant and diverse organosedimentary structures as well as the highest mineralization intensities of those observed in the stream, with tufa microbialites reaching 5 cm in height (Figure 3h,i). In the less hydrodynamic areas of the stream (i.e., where the river bank is convex, toward the edge and in a secondary lateral channel), thick dark gelatinous slime deposits covered both soft and hard substrates. Widespread tufa microbialites were observed along the entire Zone 3 and they covered all substrates, including the coarsest components such as boulders pebbles, and cobbles regardless of the nature of the substrate. Tufa microbialites were well developed on the experimental terracotta bricks and displayed continuous mineralized crusts (up to 2 cm-thick) that had formed during 18 months of deployment in the stream (Figure 7e–j). Tufa microbialites started with micritic laminae followed by alternating loose and dense filamentous laminae. Tufa microbialites were frequently covered by blue–green biofilms and/or brown filamentous mats during the warmest time of the year (Figure 3d,f). Larval housings and pupal cases were frequently associated with the tufa microbialites (Figure 4d,e).



**Figure 10.** Main characteristics of Zone 3 from the footbridge to the point of confluence with the river (see Figure 2 for exact location). (a) View and (b) drawing of the bottom sediment mainly composed of coarse (pebble to block) material encrusted by tufa microbialites; (c) single channel (20 cm-deep) with high-velocity current and small topographic break; (d) fragment of wood encrusted by a mm-thick tufa microbialite; (e) fragments of iron encrusted by tufa microbialite; (f) shard of glass (broken bottle) without tufa microbialite during the first field campaign (October 2016); (g) tufa microbialites developed on the same glass shard (October 2018).

## 5. Discussion

### 5.1. External Controlling Processes on Mineralization

The formation of tufa in freshwater systems has been linked to several hydrogeological/physicochemical ( $p\text{CO}_2$ ,  $SI_{\text{calc}}$ , temperature, light, substrate,  $\text{Ca}^{2+}$ , etc.) and climatic, geomorphological and geological factors, e.g., [10,18,56–58]. Abiotic processes dominate tufa formation by governing the intensity, nature, and texture of the mineralization. However, the establishment and growth of tufa could also comprise a biological part and, in this case of the present investigation, may have resulted from the complex interplay between biotic and abiotic processes (see discussion in Manzo et al. [4]). The supersaturation of the water with respect to calcite ( $SI_{\text{calc}}$ ) is the most mandatory to trigger mineral precipitation processes in freshwater settings [18] that can lead to the formation of tufa [4].  $SI_{\text{calc}}$  is strongly influenced by the variation of the partial pressure of  $\text{CO}_2$  ( $p\text{CO}_2$ ) [57].

In the tributary of the Mérintaise River, the distribution of tufa microbialite all along the stream may be explained by the evolution of these two parameters (Figure 11a). Except the first few hundred meters close to the source (the first part of Zone 1), the water is generally supersaturated with respect to calcite ( $SI_{\text{calc}} > 0$ ), gradually increasing downstream. However, no mineralization was observed in the last part of zone 1, in spite of a positive  $SI_{\text{calc}}$ , ranging between 0.4 and 0.5. Spontaneous calcite precipitation is reported to start from about 10-fold the supersaturation (0.8 to 1.1), see, e.g., [18,56,57,59]. If so,  $SI_{\text{calc}}$  probably prevented mineralization in this part of the stream. The non- or low-supersaturation with respect to calcite is typically linked to low pH values (<8), which also prevent the precipitation of calcite [60]. Low pH values in the entire Zone 1 result from one or several processes associated with the reed-dominated vegetation, including degradation of organic matter and respiration of roots causing uptake of soil-originated  $\text{CO}_2$ , and decrease the pH [56]. Downstream, in Zones 2 and 3 that were dominated by forest, the pH was generally above 8, with the highest average values in Zone 3. The increasing pH and  $SI_{\text{calc}}$  values coincide with the decrease in  $p\text{CO}_2$  values (the calcium concentration and alkalinity values remain stable; Table 3; Figure 2).  $\text{CO}_2$  degassing, either from physical or biological processes, is one of the most frequently discussed factors in the literature to explain the development of tufa by favoring the mineralization of calcite, see, e.g., [5,52,61–64]. Physical  $\text{CO}_2$  degassing may occur in fast flowing or turbulent waters and/or in a system with high DIC concentrations. Consequently, tufas typically grow faster in high-energy settings with intense degassing, e.g., [5,61,63,65,66]. Several topographic breaks, such as the outlets of the water pipe in Zone 1 and the numerous turbulent areas in Zone 3 caused the mechanical  $\text{CO}_2$  degassing from the stream. Tufa microbialites were present in the fast-flowing zones (e.g., Zone 3), where the channel is single and the vegetation dominated by forest (Figure 9). In contrast, tufa formation was not observed in the slow-flowing, multi-channel reed-dominated part of the stream. Slight variations of some chemical parameters in Zone 3 were observed and may be the result of local groundwater input along the stream, increasing the  $p\text{CO}_2$  and decreasing in  $SI_{\text{calc}}$  values, as observed in Mesa and Piedra rivers [64,67].

Biological  $\text{CO}_2$  uptake through photosynthesis by microorganisms may contribute to  $\text{CO}_2$  removal from the stream [18,61,62,68,69]. The respective contribution of each process to  $\text{CO}_2$  removal is impossible to assess [64], but some authors have estimated that cyanobacterial photosynthesis (e.g., by *Rivularia*) may account for up to 20% of the total  $\text{CO}_2$  removal [70] and 10–20% of the total  $\text{Ca}^{2+}$  loss [5]. While the process of photosynthesis is often considered less efficient than physical  $\text{CO}_2$  degassing [52,58,66], it should not be neglected, depending on the hydrodynamic conditions. Furthermore, the  $\text{CO}_2$  uptake by photosynthesis can contribute more than mechanical  $\text{CO}_2$  removal under slow flowing conditions [18,61,62,68,71], which mimic the prevailing hydrodynamics in the stream investigated in this study. The microbial mats and biofilms composed of diatoms, cyanobacteria, filamentous algae and/or chemolithoautotrophic bacteria were present along the stream and can participate in the photosynthetic removal of carbonate species from water, lowering the  $p\text{CO}_2$ . In fact, the exchange of pore water from microbial mats and EPS matrices is slow and  $\text{CO}_2$  removal by microbes is typically very fast in these benthic ecosystems, resulting in extreme local pH value (e.g.,  $\text{pH} > 11$ ) [72]. In addition, macrophytes and reed beds may also contribute to  $\text{CO}_2$  removal from the water column [73]. The tufa microbialites were more abundant and thicker in Zone 3, where the diversity and abundance of microbial mats and biofilms was higher. Conversely, Zone 1 displayed less diversity of microbial mats and biofilms and consequently did not support tufa development.



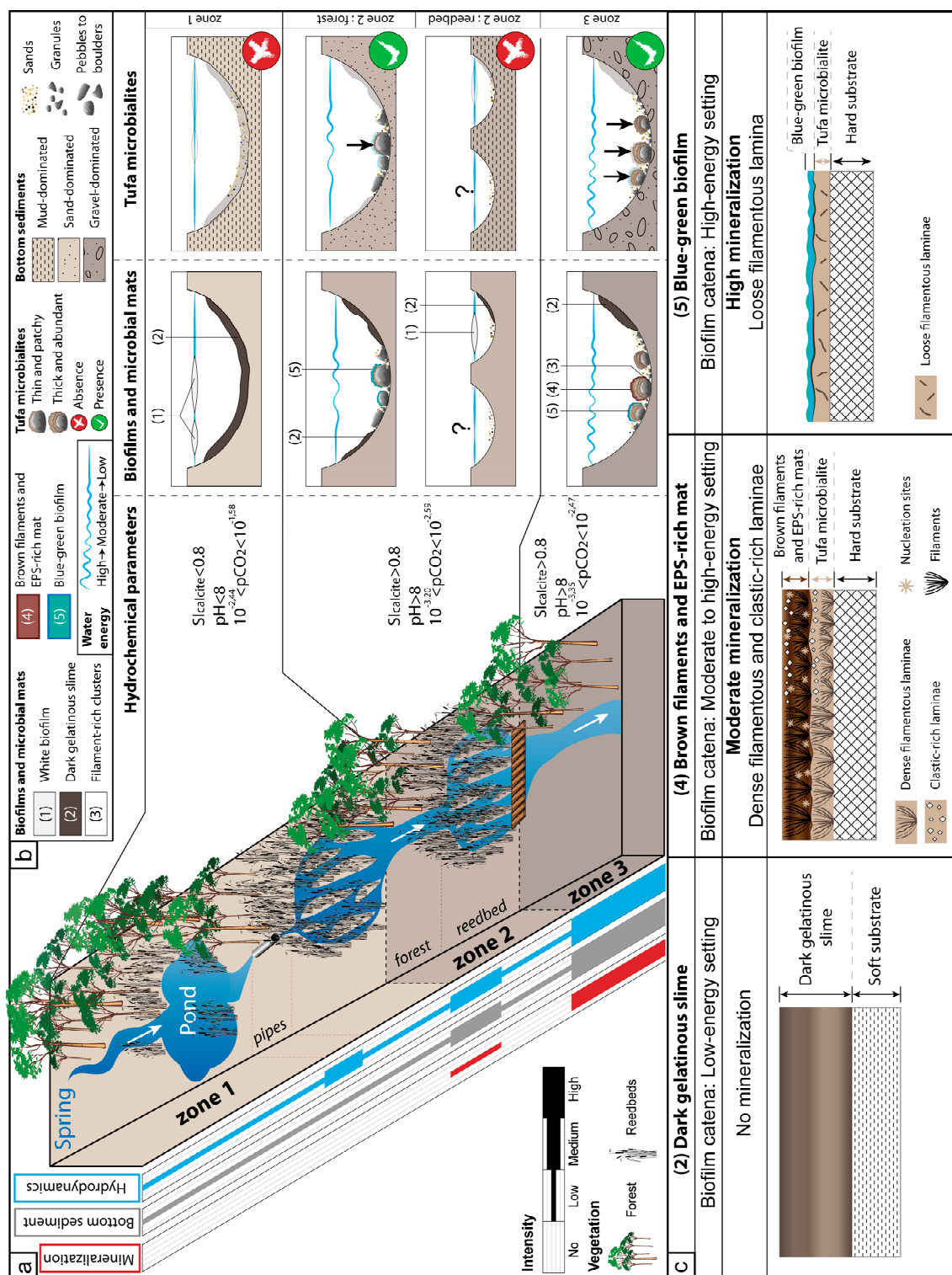


**Figure 11.** Diagram depicting the main biotic and abiotic characteristics: (a) Development of microbial mats, biofilms, and tufa microbialites along the stream showing the distribution of the bottom sediment, hydrodynamics, and the degree of mineralization; (b) detail of the channel bottom for each zone showing the development of living microbial mats and biofilms; note that the mineralization mainly occurred in Zone 3 and scarcely in Zone 2 as shown by the distribution of the tufa microbialites; (c) variations in degree of mineralization partly resulting from the thickness of the EPS (dark gelatinous slime/brown filaments EPS-rich mat) with an increase of mineralization observed when the EPS layers were thinner.

## 5.2. Link Between Living-Microbial and Mineralized Organosedimentary Structures

As outlined above, although abiotic processes are the major drivers that induce mineralization and tufa, biotic influences cannot be neglected. The distribution of microbial mats and biofilms is driven by the hydrodynamic conditions [11,42], which consequently impact mineralization processes, see, e.g., [10,68]. In the Mérantaise River, the development of organosedimentary structures seems correlated to the hydrodynamics of the streambed (Figure 11b). When the hydrodynamic conditions are weak, white biofilms develop at the water-air interface. The slow flow rate also supports development of a dark gelatinous slime, consisting of EPS accumulation, on the edges and at the bottom of the stream. Conceivably, this thick gelatinous slime was produced by the abundant diatom communities (e.g., *Gyrosigma*), which can produce copious amount of EPS [74]. Alternatively, but less likely, the slime can form from the accumulation of transported EPS, produced upstream [75]. In higher hydrodynamics conditions, the filamentous-rich clusters settle in cavities on the edges of pebbles or cobbles, which were protected from the high-energy regime. Some biofilms [76] and EPS-rich mats [42,77,78] are easily damaged and disintegrate when water flow is too fast. The white biofilm, gelatinous slime and filament-rich clusters, observed along the entire stream from Zone 1 to Zone 3, are poorly mineralized as only some micritic crystals have been observed in the dark gelatinous slime. Filamentous biofilms thrive in moderate to high-energy environments, where ciliate abundance tends to be higher than in the low-energy settings, as proposed by Primc-Habdija et al. [79]. In Zones 2 and 3, the brown filamentous mats prevail and are commonly associated with the blue-green biofilms. The latter contain diatoms of Genus *Cocconeis* and *Naviculata lanceolate*-type, which tolerate a strong current [80,81]. The presence of thin blue-green biofilms under the highest hydrodynamic conditions is consistent with stressful conditions at the bottom of the stream inhibiting other biotic components to thrive [68]. The preferentially epiphytic development on the tufa microbialites questions their role in the mineralization processes, since mineralization intensity is not homogenous within the same zone, as well as the thickness of preserved tufa microbialites.

The characteristic petrographic components of tufa are micrite, microspar and spar [4]. In the tufa microbialites from the tributary of the Mérantaise, the main evidence for mineralization was micrite and peloids, while sparite calcite crystals were absent. A biological origin for micrite has been commonly accepted [4,24], contrary to the sparry calcite, which is still considered as a pure inorganic product [27]. Large calcite crystals are common components of many physicochemically produced deposits in freshwater streams. The absence or poor development of microbial mats typically results in microcrystalline precipitation, e.g., sparry calcite [10]; palisade crystals [57]; columnar calcite spar, [82]; macrocrystalline calcite [58], as was found in the Piedra river (Spain). Thus, the widespread presence of biofilms and microbial mats covering the different substrates in the stream of the current study may explain the absence of sparite crystals. The absence of macrocrystals in our fabrics corresponds with the model proposed by Manzo et al. [4], which indicates that precipitation of sparite cannot occur when microbial mats are abundant.

The study of microstructures and their relation with biological components facilitate a better understanding of a biotic vs. abiotic origin of tufa microbialites. Even if some authors proposed a purely physicochemical role in the shape of crystals [76,83–85], the role of microorganisms has been also recognized. The precipitation of carbonates is enhanced by the presence of EPS and especially its degradation [24,29,57,86–88]. However, Pedley [68], Turner and Jones [75], Pedley and Rogerson [27] have noticed that crystals nuclei may be present in EPS without microbial cells or activity. Our SEM investigations on microbial mats and biofilms of the Mérantaise tributary stream have highlighted the role of biotic components, especially microorganisms and EPS, in the mineralization processes and the formation of tufa (Figure 5a–f). Calcite lamellas encrusting the filaments, similar to those obtained in laboratory studies [89] were observed in the tufa microbialites. The laboratory experiments, in which part of the natural community of microorganisms was present, indicated that the lamellas presented the first stage of calcium carbonate precipitation by *Phormidium* sp. The micro-peloids found in tufa microbialites of our investigation were also observed by Payandi-Rolland et al. [89], who contributed



their formation to the activity of the filamentous cyanobacteria *Oscillatoriales* sp. and EPS. The presence of numerous holes in our thin sections (Figure 4a) could be traces of *Oscillatoriales* sp.-like organisms and the micro-peloids could thus be considered as indirect evidence of microbial activity. The presence of nanostructures generally argues for a biologic tufa origin: Nanospheres have been observed in other studies, e.g., nanocrystal [4,24]; spherulites; [28,90]; nannobacteria, [91] and are viewed as fundamental structures associated with EPS or microbial activity [4,24,28,91]. The acicular dendrites found in this study resemble with long-crystallite dendrite triads [28,92], short calcite fibers [4], short triads [24], dendrite lattice [75] and dendritic calcite [90]. Pedley et al. [28] reported that dendrites were associated with cyanobacterial sheaths or green algal cell membranes, acting as catalyst for nucleation of calcite spar. The triangular polyhedra of the current study are very similar to 'short-crystallite dendrite calcite' [28]; short-calcite fibers, [4]; short triads [24]; 'saw-tooth'-like rhombohedra [90], and dendrite in a triangular domain [75]. The massive triangular polyhedra were always found in association with EPS [28], supporting a biologically-mediated origin of tufa [93].

The complex role of the community structure (e.g., changing the pH and DIC through the combined microbial metabolisms) and properties of the EPS (e.g., cation-binding capacity) affect carbonate precipitation and lithification [7,22,94]. Both changes in alkalinity and Ca-binding or release from EPS  $\text{Ca}^{2+}$  concentration are tightly coupled to metabolic activity and impact the precipitation of minerals in microbial mats [6,7]. While the characterization of the microbial communities in the stream was beyond the scope of this paper, a clear relationship exists between the thickness of the microbial mats and the intensity of mineralization. The thicker (i.e., more developed) microbial mats with copious amounts of EPS only develop under reduced hydrodynamic conditions and are associated with a low degree of mineralization (Figure 11b,c). Exactly the same pattern was observed along a lithification gradient (i.e., from completely lithified to soft mat) in a hypersaline pond in Eleuthera [23]: The lithified mats were associated with a dense community, and the non-lithifying mats with a less dense microbial community embedded in a copious/large amount of EPS. The blue-green microbial mats in high hydrodynamic conditions, in this study, were thinner and have a dense, more compact microbial community including numerous filamentous cyanobacteria (Figure 11b,c). These blue-green biofilms probably originate the loose filamentous laminae. The dense filamentous laminae are slightly less mineralized than the loose ones being enriched in micritic matrix and evidence of microbially-influenced microstructures (see previous paragraph) [7]. The copious erected filaments organized in bundles in the brown filamentous and EPS-rich mats are compared with the dense filamentous laminae of tufa microbialites. The lower mineralization products in the laminae may be related to the presence of higher EPS. While biologically stabilized, these layers are frequently reworked when the flow rate increases [77,78]. Clastic grains trapped in the dark gelatinous slime are evidence for occasional events of high episodic sediment influxes. These episodic events can have a negative impact on the growth of the tufa microbialites, either by mechanical erosion/disruption or by dissolution when acidic compounds, such as humic acids are leached into stream water, causing the decrease of  $\text{SI}_{\text{calc}}$  [67]. This scenario is consistent with clastic-rich layers composing the microfabrics of tufa microbialites and the frequent erosional surfaces observed in the current study.

### 5.3. Role of Substrate on the Spatial Distribution of Tufa

#### 5.3.1. Physical Role of the Substrate

Both physicochemical properties of water column and biological components control the mineralization processes, but they cannot explain the local variation in the degree of mineralization. As discussed above, the increasing degree of mineralization and tufa microbialites thickness along the course of the stream could also be explained by changes in hydrodynamic and chemical conditions (Figure 11a,b). However, these factors cannot explain the lack of tufa microbialite in parts of Zones 2 and 3. A main difference between areas of mineralization and those lacking mineralization are the granulometry and the nature of the bottom sediment. The tufa microbialites are mainly present

where the bottom sediment is coarser and composed of gravel and sparse boulders. In contrast, tufa microbialites are absent where muds, silt and sand predominate the streambed; only low to non-mineralized microbial mats developed (i.e., the dark gelatinous slime) in these conditions. Thus, the presence of a hard substrate (e.g., pebbles, cobbles, boulders) seem to be important in the development and preservation of tufa microbialites, as was noted in recent and fossil lacustrine (freshwater lacustrine stromatolites in Cuatros Cienegas Basin by Winsborough et al. [95]; the East African Rift by Casanova, [96], recent to Pleistocene tufas of Pyramid lake in USA by Benson [14]) and marine environments (Jurassic deep-marine microbial structures in France and Canada by Dromart et al. [13]; recent Bahamian stromatolites by Ginsburg and Planavsky [12]). Modern thrombolites (e.g., of Lake Clifton, Western Australia) may not always be anchored on a hard substrate, but a stable substrate is a minimum required for their development [97]. Both these bottom characteristics are closely related: The harder and extensive the substrate is, the more stable tends to be. The substrate stability explained the formation of microbial deposits in lacustrine setting, where an accumulation of caddisfly larval cases as supported tufa development in Papua New Guinea [98], in a modern travertine-depositing stream in Australia [99]; Eocene Green River Formation in USA [53] and in Oligo-Miocene Limagne Basin in France [100,101]. Several other studies considered the stability of the substrate as controlling factors in the development, the distribution and the morphologies of microbial deposits [102–104]. Della Porta [3] and Bouton et al. [102] suggested that stable substrates and limited disturbance were important factors governing the shape and the spatial distribution of the microbial buildups in the Great Salt Lake (USA). Dromart et al. [13] proposed that the stability of depositional surface directly determined the growth of the structure: The limited size of hard and unstable substrate resulted in the formation of oncolites or vertically poorly developed microbial mats. One of the main factors favoring lacustrine tufa development and preservation in Pyramid lake (USA) was a hard substrate [14].

In the Méranaise tributary stream, the small-sized sediments were resuspended in high hydrodynamic conditions and the dark gelatinous slime was removed. The presence of boulders and hard substrates in the hydrodynamic settings, influence the ability of microbial communities to colonize and anchor on the substrate. The filamentous nature cyanobacteria and the EPS matrix directly stabilize biofilms and microbial mats [11,105]. Early lithification of the blue–green microbial mats and the brown filamentous EPS-rich mats contributed to the stabilization and formation of a new lithified substrate. This allowed formation of loose (associated with blue–green mats) and dense (with brown filamentous EPS-rich mats) filamentous tufa microbialites. The thicker and more complex lithified tufas developed on hard substrates usually have a greater preservation potential [40,106,107]. The nature of the substrate surface also influences growth rate of the organosedimentary structures: A 5-mm thick mat developed in only eight months on a terracotta brick, but took two years to reach that thickness on a smooth glass surface (Figure 10 f,g). This difference in growth rate may result from the surface roughness of the surface [79]. Other studies identified that surface roughness and nature of the substrate as major were factors in colonization rate and species composition [108–111].

### 5.3.2. Chemical Role of the Substrate

In the Méranaise tributary stream, all hard substrates are colonized regardless of their anthropogenic or sedimentological composition (e.g., chert, wood, brick, glass or iron). However, the chemical composition of the substrate may impact the colonization by microbial communities, the ability to mineralize and preservation potential. During the development of tufa microbialite, the nature of the initial layer may depend on its chemical composition of the underlying substrate. For example, an iron-rich initial layer is typically observed on iron substrates (Figures 3i and 6b,c). Numerous investigations highlighted the composition of the substrate in determining the development of the tufa [10,15–21]. Gradzinski [10] showed for example that tufa grew faster on a limestone substrate than on copper, confirming the toxicity of the latter. The toxicity of the copper for the micro-organisms is well known (Cu toxicity) and delays the algae and cyanobacteria colonization [112,113]. Metal exposure may increase the production of EPS and change the relative abundance of taxa in a community

depending on their species-specific response to the metals [112]. Cyanobacteria are highly effective in sorption of metals [114] and presumably the EPS is an important sink for these [25]. Consequently, iron-metabolizing organisms colonizing the Fe-rich substrate could form the base of the tufa microbialite found in this study (Figures 3i and 6b,c; see [115]). The lithified crusts covered the iron substrate, thus limiting contact and toxic effects of the substrate. This allows metal-sensitive mat-building species to colonize and form the ordinary alternating loose and dense filamentous tufa laminae. A similar scenario was proposed by Gradzinski [10], where protective calcite layers precipitated on copper surfaces supported the development of tufa.

#### 5.4. External Control on the tufa Microbialite Fabric

With the exception of an occasional initial layer, petrographic textures of tufa microbialite generally showed alternating stacking of dense filamentous and loose filamentous laminae. This couplet of dense and loose laminae was observed regardless of the position in the stream and the nature of substrates, including experimentally deployed terracotta bricks. These common tufa fabrics: Porous (dense filamentous, in this study) and dense (loose filamentous, in this study) laminae are widely documented in tufa formed in other freshwater settings, e.g., [4,10,50,56–58,76,116,117]. This couplet, also called “bioarvites” [118], is attributed to a seasonal lamination pattern [10,54,56,116,119,120] or other cyclic events (e.g., seasonal, monthly, or shorter and non-periodic processes) [58]. The alternation between different laminae has been attributed to variations in microbial growth patterns during the summer and winter months [120–123] governed by temperature, insolation [10,52,61,124], nutrient availability, or ecological interactions within the microbial community [86,125]. A abiotic-biotic combined effect can be due to the increase of temperature which favors the CO<sub>2</sub> degassing. Ultimately, this results in different carbonate precipitation rates [56,126]. Depending on the geographic settings, the seasonal pattern can be reversed, appearing dense in the summer and porous in the winter [56,58,61,116,124] or porous in the summer and dense in the winter [50,119,127].

In the microbial mats of the Méranaise tributary stream, the most common cyanobacterial taxa belong to the subclasses Oscillatoriales (e.g., *Phormidium* sp.) and Pseudanabaenales (*Leptolyngbya* sp.), as revealed by morphological (this study) and phylogenetic analyzes [89]. Two main size classes were present in the dense filamentous laminae in which the cyanobacteria are positioned vertically. The larger filaments resembled to *Oscillatoriales* sp.-like and the smaller cyanobacteria appeared related to *Leptolyngbya* sp. The loose filamentous laminae were composed of disorganized, single-sized filaments similar to *Phormidium* sp. morphology. Our observations in natural and experimental setting suggest a preferential development of dense, vertically-oriented filamentous laminae during higher temperatures (warmer seasons) that contrasts the loose filamentous laminae form during colder seasons.

The deployment of bricks along the course of the stream course clearly documented variations in the degree of mineralization from Zone 1 to Zone 3 and the seasonal pattern. Larval housings, the presence of which is used as indicator for the spring season [17,50], developed in all laminae in our study and could not be used as temporal marker. The formation of the initial micritic laminae on the bricks may have been delayed due to differences between the crystal size of the substrate and calcite precipitate [128]. Such a lag phase is commonly observed for colonization of a pioneer community [10,50]. This can explain why some bricks supported fewer or no laminae. Alternatively, laminae could be missing or thinner, resulting from emersion [10] or to high episodic sediment influxes, eroding the newly-deposited laminae [67].

## 6. Conclusions

The 1.1 km-long freshwater stream in Villiers-le-Bâcle, tributary of Méranaise river, is an excellent natural laboratory for studying changes in carbonate mineralization processes in relation to microbial activity. The development of microbial mats, and biofilms (white biofilms, dark gelatinous slime, filament-rich clusters, brown filaments and EPS-rich mats, and blue–green biofilms) and tufa microbialites were correlated to the hydrodynamics of the river. The brown filaments and EPS-rich

mats and the blue–green biofilm developed were generally associated with tufa microbialites. The distribution of the various benthic microbial structures allows to subdivide the river in three zones with no, low and high degrees of mineralization, increasing downstream. The tufa microbialites exhibit a fabric of a couplet of alternating loose to dense filamentous laminae. However, the initial layer is generally a micritic laminae, which can be replaced by an iron-rich crust when the substrate consists of an iron fragment. Clastic-rich laminae may form when hydrodynamic conditions increase.

The supersaturation of the water with respect to calcite ( $SI_{\text{calc}} > 0$ ) is considered as the fundamental condition that is required to trigger mineralization in freshwater settings, potentially leading to the formation of tufa.  $SI_{\text{calc}}$  is strongly influenced by variation in  $p\text{CO}_2$ . Even if the abiotic processes govern induction of mineralization and tufa development along the stream, biological factors played a critical role in the mineralization processes in the current study. The presence of specific microstructures and mineral fabrics (e.g., micro-peloids made up of aggregates of nanospheres, dendrites organized in pyramidal structures, trigonal or rhombohedral polyhedron) argue for a biological influence on the mineralization processes. The mineralization products consisted of the dense and loose filamentous laminae, which were arranged according to temperature: The development of dense filamentous laminae coincided with warmer seasons and, conversely, the development of the loose filamentous laminae with colder seasons. Finally, tufa microbialites are promoted by the presence of hard substrates that play a physical and chemical role in their development.

**Supplementary Materials:** The following are available online at <http://www.mdpi.com/2075-163X/9/6/359/s1>, Table S1: Measurements of major physicochemical parameters of studied points.

**Author Contributions:** Conceptualization, A.R. and E.V. investigation, A.R., E.V., I.B., A.B., D.P.-R., P.A.-S, H.C. and P.T.V.; writing—original draft preparation, A.R.; writing—review and editing, A.R., E.V., I.B., A.B., D.P.-R., P.A.-S, E.C.G., H.C. and P.T.V.; visualization, A.R; supervision, E.V and A.B.; project administration, E.V.

**Acknowledgments:** This study is a contribution from Total R&D (Supervisor; Emmanuelle Poli), the SEDS team of Biogéosciences laboratory (Dijon, France) to the I-site project UB18016-BGS-IS. E.V. and A.R. thank Aurélien Virgone for stimulating discussion. The authors express their gratitude to Eric Portier for his participation and discussion in the field. They also thank the guardian and the owner of the property to have allowed us access to the spring and for their logistic contribution on site. Authors are thanking Pascal Taubaty (Bourgogne Franche-Comté University, Dijon) for thin section preparation. The authors would like to thank the two anonymous reviewers whose work has helped to improve the manuscript.

**Conflicts of Interest:** The authors declare no conflict of interest.

## References

- Pedley, H.M. Classification and environmental models of cool freshwater tufas. *Sediment. Geol.* **1990**, *68*, 143–154. [[CrossRef](#)]
- Ford, T.D.; Pedley, H.M. A review of tufa and travertine deposits of the world. *Earth-Sci. Rev.* **1996**, *41*, 117–175. [[CrossRef](#)]
- Della Porta, G. Carbonate build-ups in lacustrine, hydrothermal and fluvial settings: Comparing depositional geometry, fabric types and geochemical signature. *Geol. Soc. Lond. Spec. Publ.* **2015**, *418*, 17–68. [[CrossRef](#)]
- Manzo, E.; Perri, E.; Tucker, M.E. Carbonate deposition in a fluvial tufa system: processes and products (Corvino Valley-southern Italy): Carbonate fluvial tufa deposition, processes and products. *Sedimentology* **2012**, *59*, 553–577. [[CrossRef](#)]
- Shiraishi, F.; Reimer, A.; Bissett, A.; de Beer, D.; Arp, G. Microbial effects on biofilm calcification, ambient water chemistry and stable isotope records in a highly supersaturated setting (Westerhöfer Bach, Germany). *Palaeogeogr. Palaeoclimatol. Palaeoecol.* **2008**, *262*, 91–106. [[CrossRef](#)]
- Visscher, P.T.; Stolz, J.F. Microbial mats as bioreactors: Populations, processes, and products. *Palaeogeogr. Palaeoclimatol. Palaeoecol.* **2005**, *219*, 87–100. [[CrossRef](#)]
- Dupraz, C.; Reid, R.P.; Braissant, O.; Decho, A.W.; Norman, R.S.; Visscher, P.T. Processes of carbonate precipitation in modern microbial mats. *Earth-Sci. Rev.* **2009**, *96*, 141–162. [[CrossRef](#)]
- Benzerara, K.; Skouri-Panet, F.; Li, J.; Ferard, C.; Gugger, M.; Laurent, T.; Couradeau, E.; Ragon, M.; Cosmidis, J.; Menguy, N.; et al. Intracellular Ca-carbonate biomineralization is widespread in cyanobacteria. *Proc. Natl. Acad. Sci. USA* **2014**, *111*, 10933–10938. [[CrossRef](#)]



9. Bougeault, C.; Vennin, E.; Durllet, C.; Muller, E.; Mercuzot, M.; Chavez, M.; Gérard, E.; Ader, M.; Virgone, A.; Gaucher, E.C. Biotic-abiotic influences on modern Ca-Si-rich hydrothermal spring mounds of the Pastos Grandes volcanic caldera (Bolivia). *Minerals*, Under revisions.
10. Gradziński, M. Factors controlling growth of modern tufa: results of a field experiment. *Geol. Soc. Lond. Spec. Publ.* **2010**, *336*, 143–191. [[CrossRef](#)]
11. Stal, L.J.; van Gernerden, H.; Krumbein, W.E. Structure and development of a benthic marine microbial mat. *FEMS Microbiol. Ecol.* **1985**, *1*, 111–125. [[CrossRef](#)]
12. Ginsburg, R.N.; Planavsky, N.J. Diversity of Bahamian Microbialite Substrates. In *Links Between Geological Processes, Microbial Activities & Evolution of Life: Microbes and Geology*; Dilek, Y., Furnes, H., Muehlenbachs, K., Eds.; Modern Approaches in Solid Earth Sciences; Springer: Dordrecht, The Netherlands, 2008; pp. 177–195. ISBN 978-1-4020-8306-8. [[CrossRef](#)]
13. Dromart, G.; Gaillard, C.; Jansa, L.F. Deep-Marine Microbial Structures in the Upper Jurassic of Western Tethys. In *Phanerozoic Stromatolites II*; Bertrand-Sarfati, J., Monty, C., Eds.; Springer: Dordrecht, The Netherlands, 1994; pp. 295–318. ISBN 978-94-011-1124-9. [[CrossRef](#)]
14. Benson, L. Carbonate deposition, Pyramid Lake subbasin, Nevada: 1. Sequence of formation and elevational distribution of carbonate deposits (Tufas). *Palaeogeogr. Palaeoclimatol. Palaeoecol.* **1994**, *109*, 55–87. [[CrossRef](#)]
15. Chafetz, H.; Rush, P.F.; Utech, N.M. Microenvironmental controls on mineralogy and habit of CaCO<sub>3</sub> precipitates: An example from an active travertine system. *Sedimentology* **1991**, *38*, 107–126. [[CrossRef](#)]
16. Emeis, K.-C.; Richnow, H.-H.; Kempe, S. Travertine formation in Plitvice National Park, Yugoslavia: chemical versus biological control. *Sedimentology* **1987**, *34*, 595–609. [[CrossRef](#)]
17. Janssen, A.; Swennen, R.; Podoor, N.; Keppens, E. Biological and diagenetic influence in Recent and fossil tufa deposits from Belgium. *Sediment. Geol.* **1999**, *126*, 75–95. [[CrossRef](#)]
18. Merz-Preiss, M.; Riding, R. Cyanobacterial tufa calcification in two freshwater streams: Ambient environment, chemical thresholds and biological processes. *Sediment. Geol.* **1999**, *126*, 103–124. [[CrossRef](#)]
19. Folk, R. Interaction between bacteria, nanobacteria, and mineral precipitation in hot springs of central Italy. *Géographie Phys. Quat.* **1994**, *48*, 233–246. [[CrossRef](#)]
20. Parsiegla, K.I.; Katz, J.L. Calcite growth inhibition by copper (II): I. Effect of supersaturation. *J. Cryst. Growth* **1999**, *200*, 213–226. [[CrossRef](#)]
21. Parsiegla, K.I.; Katz, J.L. Calcite growth inhibition by copper (II): II. Effect of solution composition. *J. Cryst. Growth* **2000**, *213*, 368–380. [[CrossRef](#)]
22. Baumgartner, L.K.; Spear, J.R.; Buckley, D.H.; Pace, N.R.; Reid, R.P.; Dupraz, C.; Visscher, P.T. Microbial diversity in modern marine stromatolites, Highborne Cay, Bahamas. *Environ. Microbiol.* **2009**, *11*, 2710–2719. [[CrossRef](#)]
23. Visscher, P.T.; Dupraz, C.; Braissant, O.; Gallagher, K.L.; Glunk, C.; Casillas, L.; Reed, R.E.S. Biogeochemistry of Carbon Cycling in Hypersaline Mats: Linking the Present to the Past through Biosignatures. In *Microbial Mats: Modern and Ancient Microorganisms in Stratified Systems*; Seckbach, J., Oren, A., Eds.; Cellular Origin, Life in Extreme Habitats and Astrobiology; Springer: Dordrecht, The Netherlands, 2010; pp. 443–468. ISBN 978-90-481-3799-2. [[CrossRef](#)]
24. Perri, E.; Manzo, E.; Tucker, M.E. Multi-scale study of the role of the biofilm in the formation of minerals and fabrics in calcareous tufa. *Sediment. Geol.* **2012**, *263–264*, 16–29. [[CrossRef](#)]
25. Sforza, M.C.; Daye, M.; Philippot, P.; Somogyi, A.; van Zuilen, M.A.; Medjoubi, K.; Gérard, E.; Jamme, F.; Dupraz, C.; Braissant, O.; et al. Patterns of metal distribution in hypersaline microbialites during early diagenesis: Implications for the fossil record. *Geobiology* **2017**, *15*, 259–279. [[CrossRef](#)] [[PubMed](#)]
26. Perri, E.; Tucker, M.E.; Słowakiewicz, M.; Whitaker, F.; Bowen, L.; Perrotta, I.D. Carbonate and silicate biomineralization in a hypersaline microbial mat (Mesaieed sabkha, Qatar): Roles of bacteria, extracellular polymeric substances and viruses. *Sedimentology* **2018**, *65*, 1213–1245. [[CrossRef](#)]
27. Pedley, H.M.; Rogerson, M. In vitro investigations of the impact of different temperature and flow velocity conditions on tufa microfabric. *Geol. Soc. Lond. Spec. Publ.* **2010**, *336*, 193–210. [[CrossRef](#)]
28. Pedley, M.; Rogerson, M.; Middleton, R. Freshwater calcite precipitates from in vitro mesocosm flume experiments: A case for biomediation of tufas. *Sedimentology* **2009**, *56*, 511–527. [[CrossRef](#)]
29. Dupraz, C.; Visscher, P.T.; Baumgartner, L.K.; Reid, R.P. Microbe–mineral interactions: early carbonate precipitation in a hypersaline lake (Eleuthera Island, Bahamas). *Sedimentology* **2004**, *51*, 745–765. [[CrossRef](#)]

30. Pomerol, C.; Afchain, C.; Labesse, C.; Rampon, G.; Renard, M.; Fédoroff, N.; Bournérias, M.; Jovet, P.; Cavelier, C.; Perreau, M.; et al. *Notice de la carte géologique de France (1/50000), feuille Rambouillet (218)*; BRGM: Orléans, France, 1975.
31. Lefebvre, K. Diagnostic et quantification des flux nappe-rivière: Modélisations hydrodynamique et géochimique du bassin versant de l'Yvette amont (France). Ph.D. Thesis, Paris-Saclay University, Orsay, France, December 2015.
32. Corcho Alvarado, J.A.; Purtschert, R.; Barbecot, F.; Chabault, C.; Rueedi, J.; Schneider, V.; Aeschbach-Hertig, W.; Kipfer, R.; Loosli, H.H. Constraining the age distribution of highly mixed groundwater using  $^{39}\text{Ar}$ : A multiple environmental tracer ( $^3\text{H}/^3\text{He}$ ,  $^{85}\text{Kr}$ ,  $^{39}\text{Ar}$ , and  $^{14}\text{C}$ ) study in the semiconfined Fontainebleau Sands Aquifer (France): CONSTRAINING THE AGE OF GROUNDWATER. *Water Resour. Res.* **2007**, *43*. [[CrossRef](#)]
33. Renard, F.; Tognelli, A. A new quasi-3D unsaturated-saturated hydrogeologic model of the Plateau de Saclay (France). *J. Hydrol.* **2016**, *535*, 495–508. [[CrossRef](#)]
34. Schneider, V. Apports de l'hydrodynamique et de la géochimie à la caractérisation des nappes de l'Oligocène et de l'Eocène et à la reconnaissance de leurs relations actuelles et passées: origine de la dégradation de la nappe de l'Oligocène (sud-ouest du bassin parisien). Ph.D. Thesis, Paris-Saclay University, Orsay, France, November 2005.
35. Gran, G. Equivalence volumes in potentiometric titrations. *Anal. Chim. Acta* **1988**, *206*, 111–123. [[CrossRef](#)]
36. Parkhurst, D.L.; Appelo, C.A.J. User's guide to PHREEQC—A computer program for speciation, reaction-path, 1D-transport, and inverse geochemical calculations. *US Geol. Surv. Water-Resour. Investig. Rep.* **1999**, *99*, 4259. [[CrossRef](#)]
37. Charlton, S.R.; Parkhurst, D.L. *PHREEQCI—A Graphical User Interface to the Geochemical Model PHREEQC*; U.S. Geological Survey: Denver, CO, USA, 2002. [[CrossRef](#)]
38. Wentworth, C.K. A scale of grade and class terms for clastic sediments. *J. Geol.* **1922**, *30*, 377–392. [[CrossRef](#)]
39. Piper, A.M. A graphic procedure in the geochemical interpretation of water-analyses. *Eos Trans. Am. Geophys. Union* **1944**, *25*, 914–928. [[CrossRef](#)]
40. Bouton, A.; Vennin, E.; Pace, A.; Bourillot, R.; Dupraz, C.; Thomazo, C.; Brayard, A.; Désaubliaux, G.; Visscher, P.T. External controls on the distribution, fabrics and mineralization of modern microbial mats in a coastal hypersaline lagoon, Cayo Coco (Cuba). *Sedimentology* **2016**, *63*, 972–1016. [[CrossRef](#)]
41. Ley, R.E.; Harris, J.K.; Wilcox, J.; Spear, J.R.; Miller, S.R.; Bebout, B.M.; Maresca, J.A.; Bryant, D.A.; Sogin, M.L.; Pace, N.R. Unexpected Diversity and Complexity of the Guerrero Negro Hypersaline Microbial Mat. *Appl. Environ. Microbiol.* **2006**, *72*, 3685–3695. [[CrossRef](#)]
42. Decho, A.W. Microbial biofilms in intertidal systems: An overview. *Cont. Shelf Res.* **2000**, *20*, 1257–1273. [[CrossRef](#)]
43. Krumbein, W.E.; Brehm, U.; Gerdes, G.; Gorbushina, A.A.; Levit, G.; Palinska, K.A. Biofilm, Biodictyon, Biomat Microbialites, Oolites, Stromatolites Geophysiology, Global Mechanism, Parahistology. In *Fossil and Recent Biofilms: A Natural History of Life on Earth*; Krumbein, W.E., Paterson, D.M., Zavarzin, G.A., Eds.; Springer: Dordrecht, The Netherlands, 2003; pp. 1–27. ISBN 978-94-017-0193-8. [[CrossRef](#)]
44. Neu, T.R. Biofilms and microbial mats. In *Biostabilization of Sediments*; Bibliotheks und Informationssystem der Carl von Ossietzky Universität: Oldenburg, Germany, 1994; pp. 9–15.
45. Noffke, N. *Geobiology Microbial Mats in Sandy Deposits from the Archean Era to Today*; Springer: Berlin, Germany; London, UK, 2010; ISBN 978-3-642-12772-4. [[CrossRef](#)]
46. Jørgensen, B.B. Distribution of colorless sulfur bacteria (*Beggiatoa* spp.) in a coastal marine sediment. *Mar. Biol.* **1977**, *41*, 19–28. [[CrossRef](#)]
47. Kelly, D.P.; Postgate, J.R.; Kelly, D.P. Biochemistry of the chemolithotrophic oxidation of inorganic sulphur. *Philos. Trans. R. Soc. Lond. B Biol. Sci.* **1982**, *298*, 499–528. [[CrossRef](#)] [[PubMed](#)]
48. Marvasi, M.; Visscher, P.T.; Casillas Martinez, L. Exopolymeric substances (EPS) from *Bacillus subtilis*: polymers and genes encoding their synthesis. *FEMS Microbiol. Lett.* **2010**, *313*, 1–9. [[CrossRef](#)]
49. Diatoms of North America. Available online: <https://diatoms.org/> (accessed on 13 May 2019).
50. Freytet, P.; Plet, A. Modern freshwater microbial carbonates: The Phormidium stromatolites (tufa-travertine) of southeastern Burgundy (Paris Basin, France). *Facies* **1996**, *34*, 219. [[CrossRef](#)]
51. Garcia-Pichel, F.; Al-Horani, F.A.; Farmer, J.D.; Ludwig, R.; Wade, B.D. Balance between microbial calcification and metazoan bioerosion in modern stromatolitic oncolites. *Geobiology* **2004**, *2*, 49–57. [[CrossRef](#)]

52. Berrendero, E.; Arenas, C.; Mateo, P.; Jones, B. Cyanobacterial diversity and related sedimentary facies as a function of water flow conditions: Example from the Monasterio de Piedra Natural Park (Spain). *Sediment. Geol.* **2016**, *337*, 12–28. [[CrossRef](#)]
53. Leggitt, V.L.; Cushman, R.A. Complex caddisfly-dominated bioherms from the Eocene Green River Formation. *Sediment. Geol.* **2001**, *145*, 377–396. [[CrossRef](#)]
54. Andrews, J.E.; Brasier, A.T. Seasonal records of climatic change in annually laminated tufas: Short review and future prospects. *J. Quat. Sci.* **2005**, *20*, 411–421. [[CrossRef](#)]
55. Kleinteich, J.; Golubic, S.; Pessi, I.S.; Velázquez, D.; Storme, J.-Y.; Darchambeau, F.; Borges, A.V.; Compère, P.; Radtke, G.; Lee, S.-J.; et al. Cyanobacterial Contribution to Travertine Deposition in the Hoyoux River System, Belgium. *Microb. Ecol.* **2017**, *74*, 33–53. [[CrossRef](#)] [[PubMed](#)]
56. Kano, A.; Matsuoka, J.; Kojo, T.; Fujii, H. Origin of annual laminations in tufa deposits, southwest Japan. *Palaeogeogr. Palaeoclimatol. Palaeoecol.* **2003**, *191*, 243–262. [[CrossRef](#)]
57. Arp, G.; Bissett, A.; Brinkmann, N.; Cousin, S.; De Beer, D.; Friedl, T.; Mohr, K.I.; Neu, T.R.; Reimer, A.; Shiraishi, F.; et al. Tufa-forming biofilms of German karstwater streams: microorganisms, exopolymers, hydrochemistry and calcification. *Geol. Soc. Lond. Spec. Publ.* **2010**, *336*, 83–118. [[CrossRef](#)]
58. Arenas, C.; Jones, B. Temporal and environmental significance of microbial lamination: Insights from Recent fluvial stromatolites in the River Piedra, Spain. *Sedimentology* **2017**, *64*, 1597–1629. [[CrossRef](#)]
59. Kawai, T.; Kano, A.; Matsuoka, J.; Ihara, T. Seasonal variation in water chemistry and depositional processes in a tufa-bearing stream in SW-Japan, based on 5 years of monthly observations. *Chem. Geol.* **2006**, *232*, 33–53. [[CrossRef](#)]
60. Kempe, S. Long-term records of CO<sub>2</sub> pressure fluctuations in fresh waters. In *Transport of Carbon and Minerals in Major World Rivers*; Mitt. Geol.-Paläont. Inst. Univ. Hamburg, SCOPE/UNEP Sonderband: Hamburg, Germany, 1982; Volume 52, pp. 91–332.
61. Arp, G.; Wedemeyer, N.; Reitner, J. Fluvial tufa formation in a hard-water creek (Deinschwanger Bach, Franconian Alb, Germany). *Facies* **2001**, *44*, 1–22. [[CrossRef](#)]
62. Chen, J.; Zhang, D.D.; Wang, S.; Xiao, T.; Huang, R. Factors controlling tufa deposition in natural waters at waterfall sites. *Sediment. Geol.* **2004**, *166*, 353–366. [[CrossRef](#)]
63. Shiraishi, F.; Okumura, T.; Takahashi, Y.; Kano, A. Influence of microbial photosynthesis on tufa stromatolite formation and ambient water chemistry, SW Japan. *Geochim. Cosmochim. Acta* **2010**, *74*, 5289–5304. [[CrossRef](#)]
64. Arenas, C.; Vázquez-Urbez, M.; Auqué, L.; Sancho, C.; Osácar, C.; Pardo, G. Intrinsic and extrinsic controls of spatial and temporal variations in modern fluvial tufa sedimentation: A thirteen-year record from a semi-arid environment. *Sedimentology* **2014**, *61*, 90–132. [[CrossRef](#)]
65. Drysdale, R.; Gillieson, D. Micro-erosion meter measurements of travertine deposition rates: a case study from Louie Creek, Northwest Queensland, Australia. *Earth Surf. Process. Landf. J. Br. Geomorphol. Group* **1997**, *22*, 1037–1051. [[CrossRef](#)]
66. Vázquez-Urbez, M.; Arenas, C.; Sancho, C.; Osácar, C.; Auqué, L.; Pardo, G. Factors controlling present-day tufa dynamics in the Monasterio de Piedra Natural Park (Iberian Range, Spain): depositional environmental settings, sedimentation rates and hydrochemistry. *Int. J. Earth Sci.* **2010**, *99*, 1027–1049. [[CrossRef](#)]
67. Auqué, L.; Arenas, C.; Osácar, C.; Pardo, G.; Sancho, C.; Vázquez-Urbez, M. Current tufa sedimentation in a changing-slope valley: The River Añamaza (Iberian Range, NE Spain). *Sediment. Geol.* **2014**, *303*, 26–48. [[CrossRef](#)]
68. Pedley, M. Ambient Temperature Freshwater Microbial Tufas. In *Microbial Sediments*; Riding, R.E., Awramik, S.M., Eds.; Springer: Berlin/Heidelberg, Germany, 2000; pp. 179–186. ISBN 978-3-662-04036-2. [[CrossRef](#)]
69. Pentecost, A. *Travertine*; Springer Science & Business Media: New York, NY, USA, 2005; ISBN 978-1-4020-3523-4.
70. Pentecost, A. Calcium Carbonate Deposition by Blue–Green Algae. Ph.D. Thesis, University College of North Wales, Bangor, UK, 1975.
71. Zhang, D.D.; Zhang, Y.; Zhu, A.; Cheng, X. Physical Mechanisms of River Waterfall Tufa (Travertine) Formation. *J. Sediment. Res.* **2001**, *71*, 205–216. [[CrossRef](#)]
72. Visscher, P.T.; Gemerden, H. van Production and Consumption of Dimethylsulfoniopropionate in Marine Microbial Mats. *Appl. Env. Microbiol.* **1991**, *57*, 3237–3242.



73. Sand-Jensen, K. Photosynthetic Carbon Sources of Stream Macrophytes. *J. Exp. Bot.* **1983**, *34*, 198–210. [[CrossRef](#)]
74. Winsborough, B.M. Diatoms and Benthic Microbial Carbonates. In *Microbial Sediments*; Riding, R.E., Awramik, S.M., Eds.; Springer: Berlin/Heidelberg, Germany, 2000; pp. 76–83. ISBN 978-3-662-04036-2. [[CrossRef](#)]
75. Turner, E.C.; Jones, B. Microscopic calcite dendrites in cold-water tufa: Implications for nucleation of micrite and cement. *Sedimentology* **2005**, *52*, 1043–1066. [[CrossRef](#)]
76. Pedley, M. Freshwater (phytoherm) reefs: The role of biofilms and their bearing on marine reef cementation. *Sediment. Geol.* **1992**, *79*, 255–274. [[CrossRef](#)]
77. Rittmann, B. Detachment from biofilms. In *Structure and Function of Biofilms*; John Wiley & Sons: New York, NY, USA, 1989; pp. 49–58.
78. Stolzenbach, K.D. Particle transport and attachment. In *Structure and Function of Biofilms*; Characklis, W.G., Wilderer, P.A., Eds.; J. Wiley & Sons: Chichester, UK, 1989; pp. 33–47. [[CrossRef](#)]
79. Primc-Habdija, B.; Habdija, I.; Plenković-Moraj, A. elka Tufa deposition and periphyton overgrowth as factors affecting the ciliate community on travertine barriers in different current velocity conditions. *Hydrobiologia* **2001**, *457*, 87–96. [[CrossRef](#)]
80. Cox, E.J. *Identification of Freshwater Diatoms from Live Material*; Chapman & Hall: London, UK, 1996; ISBN 978-0-412-49380-5.
81. Lavoie, I.; Hamilton, P.B. *Guide D'identification des Diatomées des Rivières de l'Est du Canada*; PUQ: Québec, QC, Canada, 2008; ISBN 978-2-7605-1984-8.
82. Brasier, A.T.; Andrews, J.E.; Kendall, A.C. Diagenesis or dire genesis? The origin of columnar spar in tufa stromatolites of central Greece and the role of chironomid larvae. *Sedimentology* **2011**, *58*, 1283–1302. [[CrossRef](#)]
83. Butcher, R.W. Studies in the Ecology of Rivers: VI. The Algal Growth in Certain Highly Calcareous Streams. *J. Ecol.* **1946**, *33*, 268–283. [[CrossRef](#)]
84. Golubić, S.; Marčenko, E. Über Konvergenzerscheinungen bei Standortsformen der Blaualgen unter extremen Lebensbedingungen. *Schweiz. Z. Für Hydrol.* **1965**, *27*, 207–217. [[CrossRef](#)]
85. Golubić, S. The relationship between blue–green algae and carbonate deposits. In *The Biology of Blue–green Algae*; Carr, N.G., Whitton, B.A., Eds.; Basil Blackwell: Oxford, UK, 1973; pp. 434–472.
86. Reid, R.P.; Visscher, P.T.; Decho, A.W.; Stolz, J.F.; Bebout, B.M.; Dupraz, C.; Macintyre, I.G.; Paerl, H.W.; Pinckney, J.L.; Prufert-Bebout, L.; et al. The role of microbes in accretion, lamination and early lithification of modern marine stromatolites. *Nature* **2000**, *406*, 989. [[CrossRef](#)] [[PubMed](#)]
87. Trichet, J.; Défarge, C.; Tribble, J.; Tribble, G.; Sansone, F. Christmas Island lagoonal lakes, models for the deposition of carbonate–evaporite–organic laminated sediments. *Sediment. Geol.* **2001**, *140*, 177–189. [[CrossRef](#)]
88. Dupraz, C.; Visscher, P.T. Microbial lithification in marine stromatolites and hypersaline mats. *Trends Microbiol.* **2005**, *13*, 429–438. [[CrossRef](#)] [[PubMed](#)]
89. Payandi-Rolland, D.; Roche, A.; Vennin, E.; Visscher, P.T.; Amiotte-Suchet, P.; Thomas, C.; Bundeleva, I. Carbonate precipitation in freshwater cyanobacterial biofilms forming microbial tufa. *Minerals*, Submitted.
90. Chekroun, K.B.; Rodríguez-Navarro, C.; González-Muñoz, M.T.; Arias, J.M.; Cultrone, G.; Rodríguez-Gallego, M. Precipitation and Growth Morphology of Calcium Carbonate Induced by *Myxococcus Xanthus*: Implications for Recognition of Bacterial Carbonates. *J. Sediment. Res.* **2004**, *74*, 868–876. [[CrossRef](#)]
91. Folk, R.L. Nannobacteria and the precipitation of carbonate in unusual environments. *Sediment. Geol.* **1999**, *126*, 47–55. [[CrossRef](#)]
92. Pedley, M. The morphology and function of thrombotic calcite precipitating biofilms: A universal model derived from freshwater mesocosm experiments. *Sedimentology* **2014**, *61*, 22–40. [[CrossRef](#)]
93. Rogerson, M.; Pedley, H.M.; Middleton, R. Microbial influence on macroenvironment chemical conditions in alkaline (tufa) streams: Perspectives from in vitro experiments. *Geol. Soc. Lond. Spec. Publ.* **2010**, *336*, 65–81. [[CrossRef](#)]
94. Visscher, P.T.; Reid, R.P.; Bebout, B.M.; Hoefft, S.E.; Macintyre, I.G.; Thompson, J.A. Formation of lithified micritic laminae in modern marine stromatolites (Bahamas); the role of sulfur cycling. *Am. Mineral.* **1998**, *83*, 1482–1493. [[CrossRef](#)]

95. Winsborough, B.M.; Seeler, J.-S.; Golubic, S.; Folk, R.L.; Maguire, B. Recent Fresh-Water Lacustrine Stromatolites, Stromatolitic Mats and Oncoids from Northeastern Mexico. In *Phanerozoic Stromatolites II*; Bertrand-Sarfati, J., Monty, C., Eds.; Springer: Dordrecht, The Netherlands, 1994; pp. 71–100. ISBN 978-94-011-1124-9. [[CrossRef](#)]
96. Casanova, J. Stromatolites from the East African Rift: A Synopsis. In *Phanerozoic Stromatolites II*; Bertrand-Sarfati, J., Monty, C., Eds.; Springer: Dordrecht, The Netherlands, 1994; pp. 193–226. ISBN 978-94-011-1124-9. [[CrossRef](#)]
97. Moore, L.S.; Burne, R.V. The Modern Thrombolites of Lake Clifton, Western Australia. In *Phanerozoic Stromatolites II*; Bertrand-Sarfati, J., Monty, C., Eds.; Springer: Dordrecht, The Netherlands, 1994; pp. 3–29. ISBN 978-94-011-1124-9. [[CrossRef](#)]
98. Humphreys, W.F.; Awranmik, S.M.; Jebb, M.H.P. Freshwater biogenic tufa dams in Madang Province, Papua New Guinea. *J. R. Soc. West. Aust.* **1995**, *13*. [[CrossRef](#)]
99. Drysdale, R.N. The sedimentological significance of hydropsychid caddis-fly larvae (order; Trichoptera) in a travertine-depositing stream; Louie Creek, Northwest Queensland, Australia. *J. Sediment. Res.* **1999**, *69*, 145–150. [[CrossRef](#)]
100. Bertrand-Sarfati, J.; Freytet, P.; Plaziat, J.C. Microstructures in Tertiary Nonmarine Stromatolites (France). Comparison with Proterozoic. In *Phanerozoic Stromatolites II*; Bertrand-Sarfati, J., Monty, C., Eds.; Springer: Dordrecht, The Netherlands, 1994; pp. 155–191. ISBN 978-94-011-1124-9. [[CrossRef](#)]
101. Roche, A.; Vennin, E.; Bouton, A.; Olivier, N.; Watinne, A.; Bundeleva, I.; Deconinck, J.-F.; Virgone, A.; Gaucher, E.C.; Visscher, P.T. Oligo-Miocene lacustrine microbial and metazoan buildups from the Limagne Basin (French Massif Central). *Palaeogeogr. Palaeoclimatol. Palaeoecol.* **2018**, *504*, 34–59. [[CrossRef](#)]
102. Bouton, A.; Vennin, E.; Bouille, J.; Pace, A.; Bourillot, R.; Thomazo, C.; Brayard, A.; Désaubliaux, G.; Goslar, T.; Yokoyama, Y.; et al. Linking the distribution of microbial deposits from the Great Salt Lake (Utah, USA) to tectonic and climatic processes. *Biogeosciences* **2016**, *13*, 5511–5526. [[CrossRef](#)]
103. Vennin, E.; Bouton, A.; Bourillot, R.; Pace, A.; Roche, A.; Brayard, A.; Thomazo, C.; Virgone, A.; Gaucher, E.C.; Desaubliaux, G.; et al. The lacustrine microbial carbonate factory of the successive Lake Bonneville and Great Salt Lake, Utah, USA. *Sedimentology* **2019**, *66*, 165–204. [[CrossRef](#)]
104. Vanden Berg, M.D. Domes, Rings, Ridges, and Polygons: Characteristics of Microbialites from Utah’s Great Salt Lake. *Sediment. Rec.* **2019**, *17*, 4–10. [[CrossRef](#)]
105. Paterson, D.M.; Aspden, R.J.; Visscher, P.T.; Consalvey, M.; Andres, M.S.; Decho, A.W.; Stolz, J.; Reid, R.P. Light-Dependant Biostabilisation of Sediments by Stromatolite Assemblages. *PLoS ONE* **2008**, *3*, e3176. [[CrossRef](#)]
106. Jahner, R.J.; Collins, L.B. Significance of subtidal microbial deposits in Shark Bay, Australia. *Mar. Geol.* **2011**, *286*, 106–111. [[CrossRef](#)]
107. Bailey, J.V.; Orphan, V.J.; Joye, S.B.; Corsetti, F.A. Chemotrophic Microbial Mats and Their Potential for Preservation in the Rock Record. *Astrobiology* **2009**, *9*, 843–859. [[CrossRef](#)]
108. Tuchman, M.L.; Stevenson, R.J. Comparison of clay tile, sterilized rock, and natural substrate diatom communities in a small stream in Southeastern Michigan, USA. *Hydrobiologia* **1980**, *75*, 73–79. [[CrossRef](#)]
109. Lambert, G.A.; Resh, V.H. Distribution of benthic algae and macroinvertebrates along a thermal stream gradient. *Hydrobiologia* **1985**, *128*, 13–21. [[CrossRef](#)]
110. Harmsworth, G.C.; Sleigh, M.A. Colonization of non-living surfaces in streams by peritrich ciliates. *Eur. J. Protistol.* **1993**, *29*, 294–301. [[CrossRef](#)]
111. Hellal, J.; Michel, C.; Barsotti, V.; Laperche, V.; Garrido, F.; Joulain, C. Representative sampling of natural biofilms: influence of substratum type on the bacterial and fungal communities structure. *SpringerPlus* **2016**, *5*, 822. [[CrossRef](#)] [[PubMed](#)]
112. García-Meza, J.V.; Barrangue, C.; Admiraal, W. Biofilm formation by algae as a mechanism for surviving on mine tailings. *Environ. Toxicol. Chem.* **2005**, *24*, 573–581. [[CrossRef](#)] [[PubMed](#)]
113. Baptista, M.S.; Vasconcelos, M.T. Cyanobacteria Metal Interactions: Requirements, Toxicity, and Ecological Implications. *Crit. Rev. Microbiol.* **2006**, *32*, 127–137. [[CrossRef](#)] [[PubMed](#)]
114. Bender, J.; Rodriguez-Eaton, S.; Ekanemesang, U.M.; Phillips, P. Characterization of metal-binding biofloculants produced by the cyanobacterial component of mixed microbial mats. *Appl. Env. Microbiol.* **1994**, *60*, 2311–2315.

115. Konhauser, K.O.; Ferris, F.G. Diversity of iron and silica precipitation by microbial mats in hydrothermal waters, Iceland: Implications for Precambrian iron formations. *Geology* **1996**, *24*, 323–326. [[CrossRef](#)]
116. Kawai, T.; Kano, A.; Hori, M. Geochemical and hydrological controls on biannual lamination of tufa deposits. *Sediment. Geol.* **2009**, *213*, 41–50. [[CrossRef](#)]
117. Kano, A.; Hagiwara, R.; Kawai, T.; Hori, M.; Matsuoka, J. Climatic Conditions and Hydrological Change Recorded in a High-Resolution Stable-Isotope Profile of a Recent Laminated Tufa on a Subtropical Island, Southern Japan. *J. Sediment. Res.* **2007**, *77*, 59–67. [[CrossRef](#)]
118. Gerdes, G.; Krumbein, W.E.; Reineck, H.E. Biolaminations—Ecological versus depositional dynamics. In *Cycles and Events in Stratigraphy*; Springer: Berlin, Germany; New York, NY, USA, 1991; pp. 592–607.
119. Chafetz, H.S.; Folk, R.L. Travertines; depositional morphology and the bacterially constructed constituents. *J. Sediment. Res.* **1984**, *54*, 289–316. [[CrossRef](#)]
120. Dupraz, C.; Fowler, A.; Tobias, C.; Visscher, P.T. Stromatolitic knobs in Storr’s Lake (San Salvador, Bahamas): A model system for formation and alteration of laminae. *Geobiology* **2013**, *11*, 527–548. [[CrossRef](#)] [[PubMed](#)]
121. Monty, C.L.V. Chapter 5.1 The Origin and Development of Cryptalgal Fabrics. In *Developments in Sedimentology*; Walter, M.R., Ed.; Elsevier: Amsterdam, The Netherlands; Oxford, UK; New York, NY, USA, 1976; Volume 20, pp. 193–249. [[CrossRef](#)]
122. Chafetz, H.S.; Utech, N.M.; Fitzmaurice, S.P. Differences in the delta <sup>18</sup>O and delta <sup>13</sup>C signatures of seasonal laminae comprising travertine stromatolites. *J. Sediment. Res.* **1991**, *61*, 1015–1028. [[CrossRef](#)]
123. Konhauser, K.O.; Phoenix, V.R.; Bottrell, S.H.; Adams, D.G.; Head, I.M. Microbial–silica interactions in Icelandic hot spring sinter: possible analogues for some Precambrian siliceous stromatolites. *Sedimentology* **2001**, *48*, 415–433. [[CrossRef](#)]
124. Golubić, S.; Violante, C.; Plenković-Moraj, A.; Grgasović, T. Travertines and calcareous tufa deposits: An insight into diagenesis. *Geol. Croat.* **2008**, *61*, 363–378. [[CrossRef](#)]
125. Reid, R.P.; James, N.P.; Macintyre, I.G.; Dupraz, C.P.; Burne, R.V. Shark Bay stromatolites: Microfabrics and reinterpretation of origins. *Facies* **2003**, *49*, 299. [[CrossRef](#)]
126. Kano, A.; Fujii, H. Origin of the gross morphology and internal texture of tufas of Shirokawa Town, Ehime Prefecture, southwest Japan. *J. Geol. Soc. Jpn.* **2000**, *106*, 397–412. [[CrossRef](#)]
127. Melón, P.; Alonso-Zarza, A.M. The Villaviciosa tufa: A scale model for an active cool water tufa system, Guadalajara (Spain). *Facies* **2018**, *64*. [[CrossRef](#)]
128. Pentecost, A.; Coletta, P. The role of photosynthesis and CO<sub>2</sub> evasion in travertine formation: a quantitative investigation at an important travertine-depositing hot spring, Le Zitelle, Lazio, Italy. *J. Geol. Soc.* **2007**, *164*, 843–853. [[CrossRef](#)]



© 2019 by the authors. Licensee MDPI, Basel, Switzerland. This article is an open access article distributed under the terms and conditions of the Creative Commons Attribution (CC BY) license (<http://creativecommons.org/licenses/by/4.0/>).